Published OnlineFirst January 26, 2010; DOI:10.1158/0008-5472.CAN-09-3662

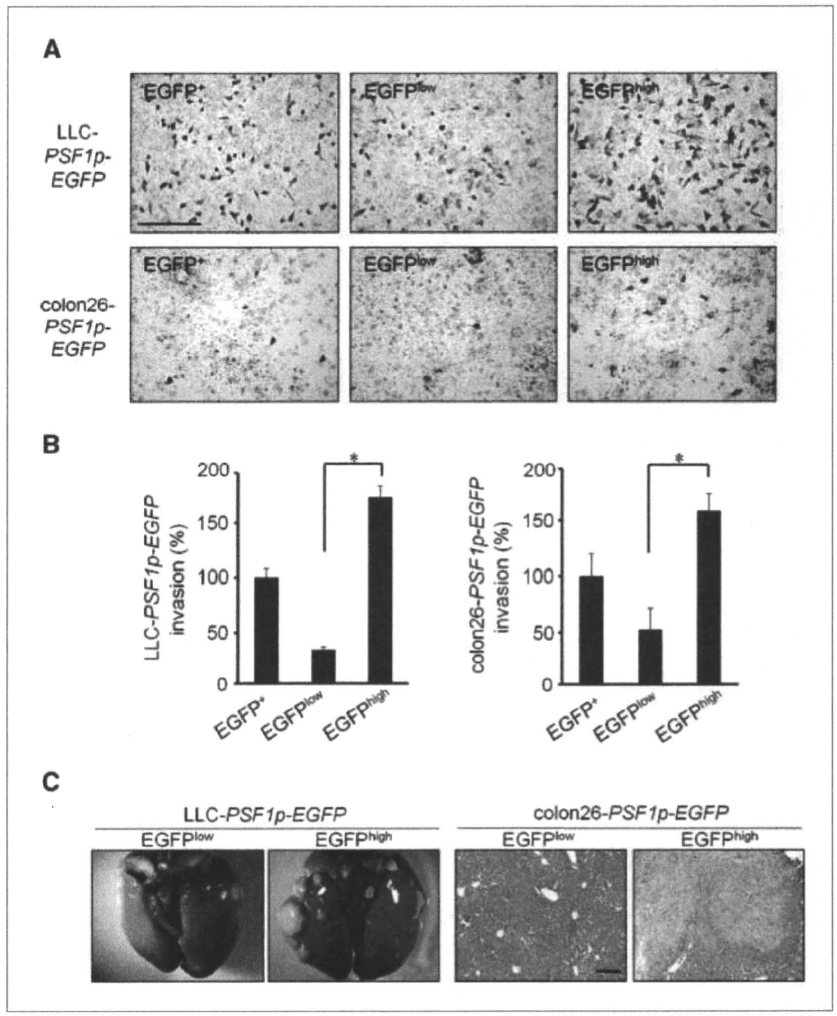

Figure 3. Invasive and metastatic capacity of LLC-*PSF1p-EGFP* and colon26-*PSF1p-EGFP*. A, representative images of sorted cells that migrated across a Matrigel-coated membrane. Bar, 200 μm. B, quantitative evaluation of the migrated cells: percentage of migrated cells relative to the applied total cell number normalized with the data from $EGFP^+$ cells. Data show the mean ± SEM. *, $P < 0.01$ ($n = 3$). Results shown are representative of at least three independent experiments. C, metastasis analysis. Gross appearance of lung metastases after injection with sorted $EGFP^{low}$ or $EGFP^{high}$ cells from LLC tumor (left). Liver metastases after injection with sorted $EGFP^{low}$ or $EGFP^{high}$ cells from colon26 tumor (right). Bar, 200 μm. Results shown are representative of at least three independent experiments.

in the lung were enumerated. Results clearly indicated that $EGFP^{high}$ cells had a higher metastatic potential than did $EGFP^{low}$ cells (Fig. 3C; Supplementary Fig. S2A). Second, in the case of colon26 tumors, viable sorted $EGFP^{high}$ or $EGFP^{low}$ cells were injected into the spleen. After 12 days, metastatic nodules in the liver were analyzed on liver sections. $EGFP^{low}$ cells rarely generated metastatic foci, but large lesions were frequently observed in the livers of mice injected with $EGFP^{high}$ cells (Fig. 3C; Supplementary Fig. S2B).

ESC-like signatures are enriched in $EGFP^{high}$ cells versus EGFPlow cells. Recent studies showed that poor prognosis in a diverse set of human and mouse malignancies is associated with the expression of an ESC-like genetic program (18). We therefore compared the gene expression signatures of $EGFP^{low}$ and $EGFP^{high}$ cells. Data clearly indicated that ESC-like signatures were enriched in $EGFP^{high}$ cells versus $EGFP^{low}$ cells (Fig. 4). Interestingly, other ESC-like signatures (24, 25), in which some cancer-initiating/stem cells (CIC/CSC) were enriched, were also enriched in $EGFP^{high}$ cells versus $EGFP^{low}$ cells (Fig. 4; Supplementary Table S1). Taken together, the results from all the above experiments lead us to conclude that cancer cells harboring large amounts of PSF1 or high transcriptional activity of *PSF1* possess malignant features, including high proliferative capacity, tumorigenesis, metastatic ability, and genetic profiles of poor prognosis.

$PSF1^{high}$ cells are localized in perivascular regions. Next, the tissue distribution of $EGFP^{high}$ cells in tumors was examined (Fig. 5A–C). $EGFP^{high}$ cells were located close to the edge of the tumor and near the blood vessels. Preliminary, we investigated PSF1 expression in human carcinoma specimens (Supplementary Fig. S3). We found that PSF1 expression in human lung and esophageal squamous cell carcinoma specimens was confined to the surrounding basal-like cells and located at some distance from the centers of terminal differentiation zones. Furthermore, PSF1-positive cells were located in close proximity to blood vessels near the edge of the tumor, as observed in our murine xenograft model (Supplementary Fig. S3).

Silencing of PSF1 inhibits the proliferation of carcinoma cells. Targeted disruption of PSF1 led to embryonic lethality

Published OnlineFirst January 26, 2010; DOI:10.1158/0008-5472.CAN-09-3662

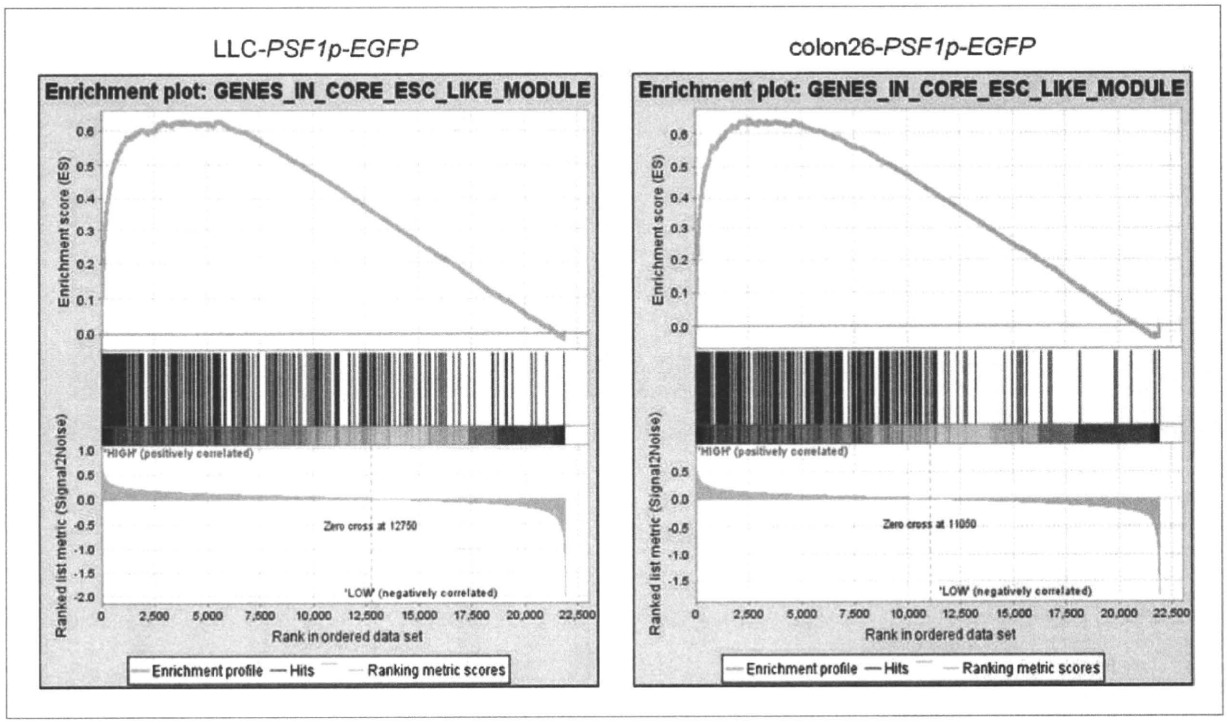

Figure 4. Gene set enrichment analysis. GSEA plots show that expression of an ESC-like core gene module (24) is more enriched in EGFP^{high} cells compared with EGFP^{low} cells in LLC-*PSF1p-EGFP* tumor and colon26-*PSF1p-EGFP* tumor.

caused by the inhibition of cell growth in the inner cell mass (12), suggesting that silencing this gene may also inhibit tumor cell proliferation. To determine whether PSF1 could be a suitable molecular target for anticancer drug development, the inhibitory effects of its expression in human carcinoma cell lines should be evaluated. In budding yeast, it has been suggested that PSF1 plays a role in DNA replication, associated with the formation of the DNA replication fork (7–9). However, its function in mammalian cells has not been clarified. First, we established the cellular localization of PSF1 in HeLa cells (Fig. 6A). At interphase, PSF1 was localized predominantly in the nuclei. During mitosis, it was almost exclusively diffusely located outside the chromatin. Next, we used short hairpin RNA (shRNA) expression plasmids for RNAi-mediated endogenous gene silencing in HeLa cells *in vitro*. Quantitative RT-PCR with gene-specific shRNA confirmed that endogenous PSF1 gene expression was reduced by more than 75% within 72 hours, compared with the lack of effect of transfection of a scrambled shRNA expression plasmid (data not shown). At 96 hours, the total number of PSF1 shRNA–treated cells was significantly decreased compared with the control (Fig. 6B), suggesting that depletion of PSF1 had resulted in cell growth arrest. To analyze more precisely the effect of PSF1 depletion on cell growth, first, the DNA contents were analyzed (Fig. 6C, left). Results showed that depletion of PSF1 led to an increase in the fraction of cells in the sub-G_1, S, and G_2-M phases, suggesting that this molecule is important not only for S phase but also for G_2-M phase progression.

Polyploid cells can arise as a result of errors in mitosis. These cells usually exit the cycle in an aberrant fashion, without sister chromatid segregation or cytokinesis, a process known as "mitotic slippage." Cancer cell lines (such as HeLa and HEK293T cells) lacking functional p53 progress into S phase without p53-dependent growth arrest at the subsequent G_1-S boundary, and hyperploid cells develop as a result. However, no obvious hyperploid cell populations were found in PSF1-depleted cells (Fig. 6C, left). During a 4-hour pulse, approximately 75% of scrambled shRNA–treated cells incorporated BrdUrd (Fig. 6C, right), but only approximately 23% of PSF1-depleted cells possessed large nuclei staining with anti-BrdUrd antibody. Taken together, these data indicate that PSF1 depletion also inhibits DNA synthesis of multiploid cells, which resulted in the generation of only a small number of cells harboring large nuclei (8N; Fig. 6C, left).

During the 72- to 120-hour period after shRNA treatment, the population of G_2-M phase cells increased in the PSF1 depletion experiments (Fig. 6C, left). Therefore, we assessed the function of PSF1 in G_2-M progression. In the scrambled shRNA–treated control population, most cells had divided within 60 minutes, whereas division times were prolonged in the PSF1-depleted cells (Fig. 6D, left). To examine this in terms of chromosome segregation, real-time imaging was done with histone H2B-GFP, which labels the chromosomes (Fig. 6D, middle). In control cells, the chromosomes were condensed and congressed to the metaphase plate, but subsequently, and suddenly, they completely segregated and the

Published OnlineFirst January 26, 2010; DOI:10.1158/0008-5472.CAN-09-3662

time spent in metaphase was between 15 and 30 minutes. By contrast, PSF1 depletion prolonged the duration of metaphase by between 33 and 145 minutes, and a proportion of the PSF1-depleted cells showed abnormal chromosome congression and segregation (data not shown). Real-time observation with GFP-tubulin also revealed that depletion of PSF1 caused arrest at metaphase (data not shown). To resolve whether this mitotic arrest, induced by PSF1 depletion, was dependent on the spindle assembly checkpoint, Mad2 was co-depleted from the cells. We found that the mitotic arrest of almost all co-depleted cells was rescued by the early onset of anaphase (Fig. 6D, right). Taken together, these data showed that, in the absence of PSF1, the spindle checkpoint signal was activated and mitotic arrest was precipitated.

Because we observed abnormalities in metaphase arrest and DNA segregation in PSF1-depleted cells, we next analyzed spindle organization by staining for β-tubulin. Results showed that approximately 10% of the mitotic cells formed multipolar asters (Fig. 6E, left), whereas a small number of abnormal spindles were found in the control experiments (data not shown). Moreover, by immunostaining with anti-survivin antibody, we found that unaligned chromosomes were present in PSF1 shRNA–treated cells, which may reflect a defect in chromosome congression or segregation (Fig. 6E, middle). Recently, we reported that PSF1-deficient mice were nonviable at around embryonic day E6.5 and that BrdUrd incorporation was inhibited in the cultured inner cell mass from the blastocysts of E3.5 *PSF1*$^{-/-}$ embryos (12). Consistent with the present results from RNAi experiments in HeLa cells, we found that micronuclei and abnormal chromosomal segregation occurred in E3.5 *PSF1*$^{-/-}$ blastocysts (Fig. 6E, right). These data indicate that PSF1 contributes not only

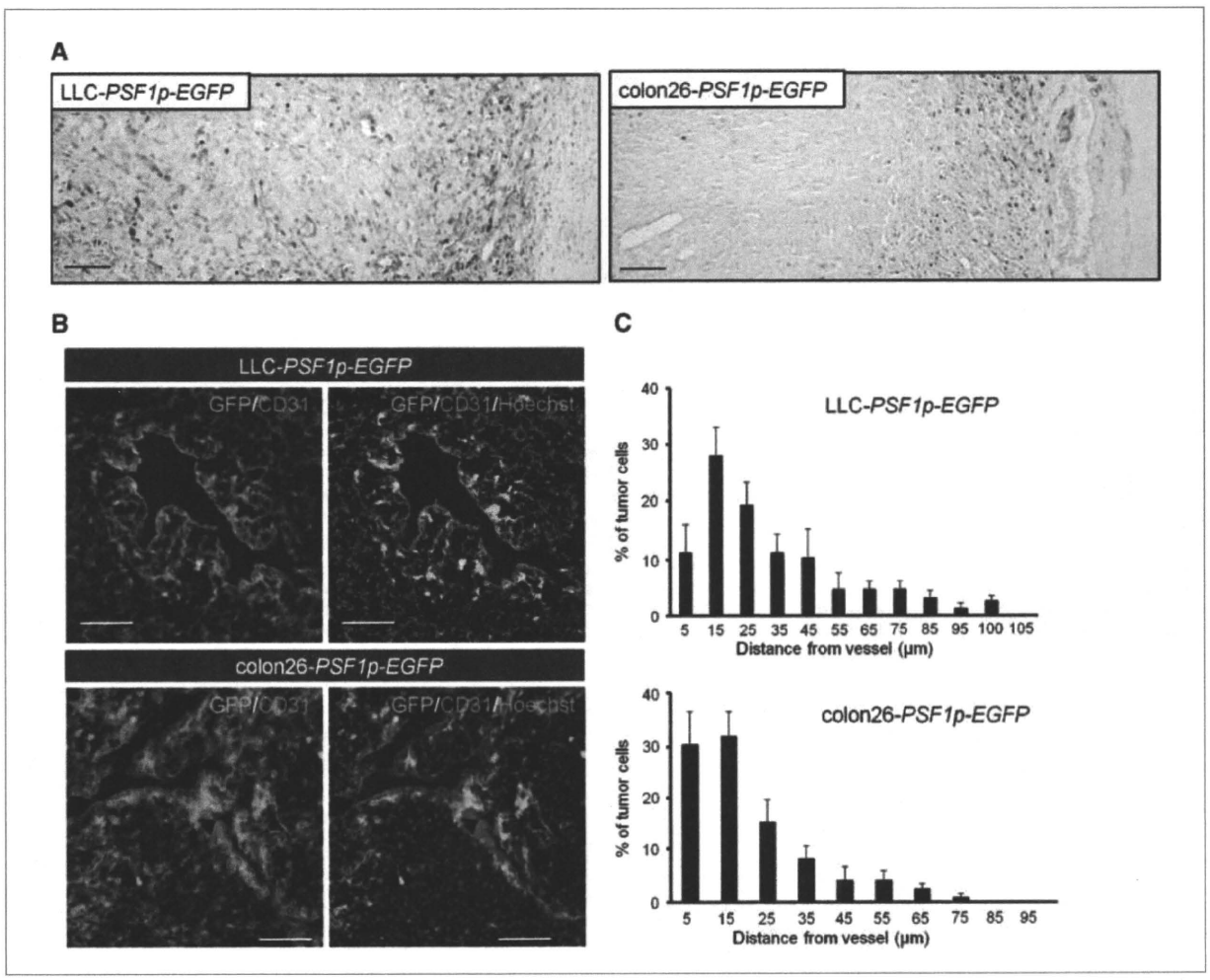

Figure 5. Localization of cancer cells strongly expressing PSF1. A, sections from LLC-*PSF1p-EGFP* (left) and colon26-*PSF1p-EGFP* (right) xenografts were double stained with anti-GFP antibody (brown in left, purple in right) and anti-CD31 antibody (red). Bar, 100 μm. B, sections of LLC-*PSF1p-EGFP* (top) and colon26-*PSF1p-EGFP* (bottom) tumor tissues were stained with anti-CD31 antibody (red). Nuclei were counterstained with Hoechst 33342 (blue). Endogenous EGFP was observed in low contrast (left) and high contrast (right). C, percentages of EGFP^{high} cells that were located at incremental distances of 5 μm from the nearest CD31^{+} endothelial cells. Data are mean ± SEM from five random fields. Bar, 100 μm.

Published OnlineFirst January 26, 2010; DOI:10.1158/0008-5472.CAN-09-3662

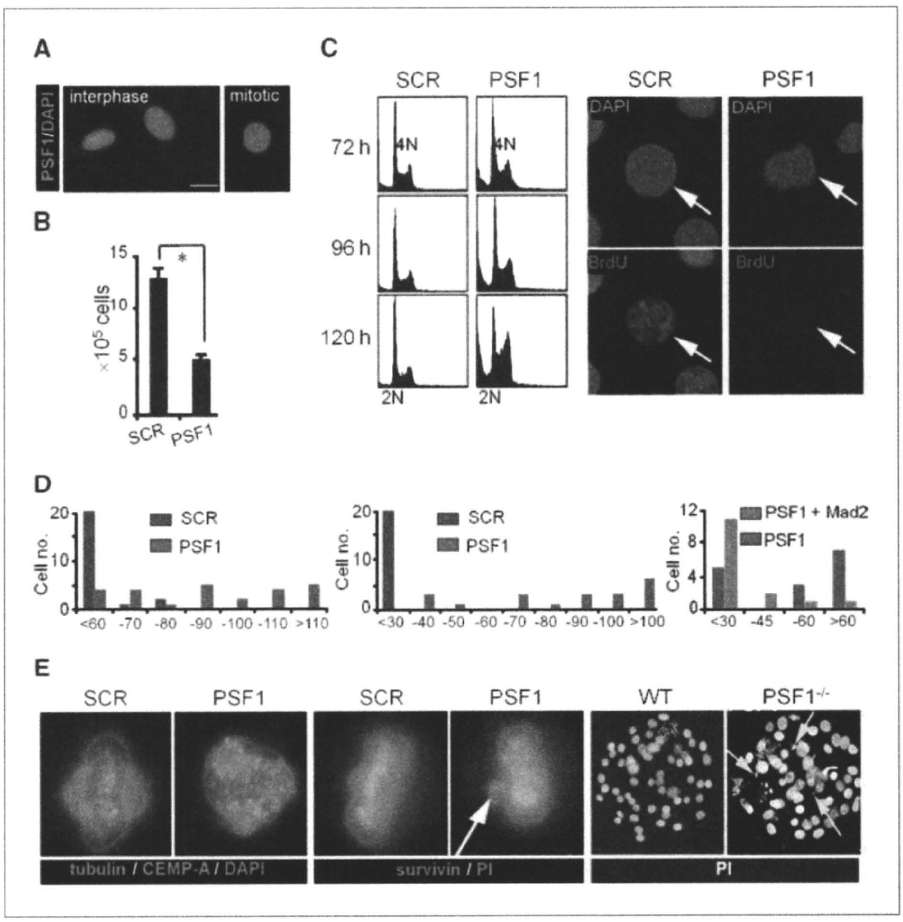

Figure 6. *PSF1* silencing inhibits proliferation of cancer cells. A, HeLa cells were immunostained with anti-PSF1 (green). DNA was counterstained with 4′,6-diamidino-2-phenylindole (DAPI; blue). B, total numbers of RNAi-treated HeLa cells 96 h after transfection (bottom). *SCR*, nonspecific scrambled shRNA as a negative control. *, $P < 0.05$. C, DNA content of shRNA-treated HeLa cells (72 h after transfection) was determined by flow cytometry (left). DNA synthesis in large nucleated cells treated with the indicated shRNA. Immunostaining was done with anti-BrdUrd antibody (red), and counterstaining with DAPI (blue; right). Arrows, large nuclei. D, HeLa cells were treated with control (blue) or PSF1 (red) shRNA. Time required for cell division was evaluated by time-lapse observation 72 to 96 h after transfection (left). Using histone H3-GFP–expressing HEK293T cells, metaphase retention time was observed 72 to 120 h after transfection (middle). The H3-GFP-HEK293T cells were cotransfected with PSF1 shRNA and scrambled shRNA (red) or PSF1 and Mad2 shRNA vectors (green), and metaphase retention time was observed 36 to 72 h after transfection (right). E, HeLa cells transfected with shRNA as indicated. Expression of tubulin (green) and CENP-A (red; left). DNA was counterstained with DAPI (blue). Expression of survivin (green; middle). DNA was counterstained with propidium iodide (red). E3.5 $PSF1^{+/+}$ or $PSF1^{-/-}$ embryos were fixed and stained with propidium iodide (right). Arrows, disorganized micronuclei.

to DNA replication but also to the transition from metaphase to anaphase, as well as to chromosome segregation.

Discussion

In the present work, we used cells with a high level of expression of PSF1 to show that these malignant cancer cells, which are located in the vascular region and at the edge of the tumor, exhibit high tumorigenic and metastatic ability.

Thus far, acquisition of genetic changes affected by epigenetic manipulation and microenvironmental exposure has been suggested to be responsible for tumor progression. When we cultured the tumor cells *in vitro*, we observed that the population consisted of PSF1(EGFP)^{high} and PSF1(EGFP)^{low} fractions. When sorted and separately injected into mice, we failed to detect any marked differences between them in terms of tumorigenic or metastatic capacity (data not shown). When nonfractionated tumor cells from these cultures were injected, the tumors that developed consisted of both PSF1(EGFP)^{high} and PSF1(EGFP)^{low} cells. However, when these cells extracted from tumors *in vivo* were fractionated into PSF1(EGFP)^{high} and PSF1(EGFP)^{low} and injected into mice again, then we did see clear a difference in terms of tumorigenic and metastatic capacity between the two fractions.

Our model therefore strongly supports the possibility that environmental changes *in vivo* clearly affect the features of cancer cells with regard to tumorigenicity or nontumorigenicity. Thus, this model suggested that the interaction of cancer

Published OnlineFirst January 26, 2010; DOI:10.1158/0008-5472.CAN-09-3662

cells with their microenvironment changes them into more malignant ones. In our tumor model as well as histology of human tissues, cells highly positive for PSF1 are located near blood vessels. It has been suggested that CSCs/CICs localize in the perivascular region (26), as is observed in normal organs, where stem cells are located in the vascular niche (27). Furthermore, microarray data clearly indicated that ESC-like signatures, which are reported to be enriched in CSCs/CICs fractions, were also enriched in $EGFP^{high}$ cells versus $EGFP^{low}$ cells (Fig. 4). Thus, the subpopulation of cells strongly positive for PSF1 might include the CSC/CIC fraction.

Antitumor angiogenesis is a promising approach for managing cancer patients, and many angiogenesis-disrupting agents have been developed (28). Although some agents have already been tested clinically and prolongation of survival has been confirmed, it is impossible to destroy all of the blood vessels in a tumor. Recent research in mice has suggested that the tumor repopulates from the edge region to the center after treatment with an angiogenesis-disrupting agent (28), and also that malignant tumor cells egress through remnant blood vessels at the tumor edge after inhibition of vascular endothelial growth factor signals (29). We previously reported that blood vessels in peripheral regions of tumors are well matured compared with those in the center and that they are resistant to antiangiogenic drugs (19, 30). Our data therefore strongly support the notion that cells with malignant features located near blood vessels at the tumor edge and showing resistance to angiogenesis-disrupting agents are responsible for invasion and metastasis. Our present model represents a precise analytic tool to determine whether candidate drugs directed against cells with malignant features including CSCs/CICs or blood vessels actually do suppress proliferation of cancer cells or destroy the vascular niche.

Our data clearly indicate that PSF1 plays a pivotal role in DNA replication and microtubule organization. Recently, it has been suggested that molecules homologous with those associated with DNA replication in lower species also regulate other cellular events in mammalian cells (31–33). In higher eukaryotes, a number of environmental cues affecting cell division involve DNA replication proteins that are also used by lower eukaryotes and that perform diverse functions in cytokinesis. Therefore, there is a possibility that, in addition to its role in microtubule organization, which we have shown here, plus the known part it plays in DNA replication, PSF1 may also have other cellular functions in symmetrical or asymmetrical cell division of malignant cancer cells by influencing cell structure. As we showed here, the possibility that PSF1 is expressed by malignant cancer cells, which may include CSCs or CICs, and the finding that silencing PSF1 induced cancer cell apoptosis suggest that this molecule may represent an important new target for the development of anticancer drugs.

Disclosure of Potential Conflicts of Interest

No potential conflicts of interest were disclosed.

Acknowledgments

We thank N. Fujimoto and K. Fukuhara for technical assistance, and A. Taguchi for technical assistance with the microarray analysis.

Grant Support

Japanese Ministry of Education, Culture, Sports, Science and Technology and the Japanese Society for Promotion of Science.

The costs of publication of this article were defrayed in part by the payment of page charges. This article must therefore be hereby marked *advertisement* in accordance with 18 U.S.C. Section 1734 solely to indicate this fact.

Received 10/7/09; revised 11/25/09; accepted 12/3/09; published OnlineFirst 1/26/10.

References

1. Takayama Y, Kamimura Y, Okawa M, Muramatsu S, Sugino A, Araki H. GINS, a novel multiprotein complex required for chromosomal DNA replication in budding yeast. Genes Dev 2003;17:1153–65.
2. Bauerschmidt C, Pollok S, Kremmer E, Nasheuer HP, Grosse F. Interactions of human Cdc45 with the Mcm2-7 complex, the GINS complex, and DNA polymerases δ and epsilon during S phase. Genes Cells 2007;12:745–58.
3. Gambus A, Jones RC, Sanchez-Diaz A, et al. GINS maintains association of Cdc45 with MCM in replisome progression complexes at eukaryotic DNA replication forks. Nat Cell Biol 2006;8:358–66.
4. Kanemaki M, Sanchez-Diaz A, Gambus A, Labib K. Functional proteomic identification of DNA replication proteins by induced proteolysis *in vivo*. Nature 2003;423:720–4.
5. Moyer SE, Lewis PW, Botchan MR. Isolation of the Cdc45/Mcm2-7/GINS (CMG) complex, a candidate for the eukaryotic DNA replication fork helicase. Proc Natl Acad Sci U S A 2006;103:10236–41.
6. Pacek M, Tutter AV, Kubota Y, Takisawa H, Walter JC. Localization of MCM2-7, Cdc45, and GINS to the site of DNA unwinding during eukaryotic DNA replication. Mol Cell 2006;21:581–7.
7. Chang YP, Wang G, Bermudez V, Hurwitz J, Chen XS. Crystal structure of the GINS complex and functional insights into its role in DNA replication. Proc Natl Acad Sci U S A 2007;104:12685–90.
8. De Falco M, Ferrari E, De Felice M, Rossi M, Hubscher U, Pisani FM. The human GINS complex binds to and specifically stimulates human DNA polymerase α-primase. EMBO Rep 2007;8:99–103.
9. Kamada K, Kubota Y, Arata T, Shindo Y, Hanaoka F. Structure of the human GINS complex and its assembly and functional interface in replication initiation. Nat Struct Mol Biol 2007;14:388–96.
10. Kubota Y, Takase Y, Komori Y, et al. A novel ring-like complex of *Xenopus* proteins essential for the initiation of DNA replication. Genes Dev 2003;17:1141–52.
11. Barkley LR, Song IY, Zou Y, Vaziri C. Reduced expression of GINS complex members induces hallmarks of pre-malignancy in primary untransformed human cells. Cell Cycle 2009;8:1577–88.
12. Ueno M, Itoh M, Kong L, Sugihara K, Asano M, Takakura N. PSF1 is essential for early embryogenesis in mice. Mol Cell Biol 2005;25:10528–32.
13. Han Y, Ueno M, Nagahama Y, Takakura N. Identification and characterization of stem cell-specific transcription of PSF1 in spermatogenesis. Biochem Biophys Res Commun 2009;380:609–13.
14. Ueno M, Itoh M, Sugihara K, Asano M, Takakura N. Both alleles of

Published OnlineFirst January 26, 2010; DOI:10.1158/0008-5472.CAN-09-3662

PSF1 are required for maintenance of pool size of immature hematopoietic cells and acute bone marrow regeneration. Blood 2009; 113:555–62.
15. Obama K, Ura K, Satoh S, Nakamura Y, Furukawa Y. Up-regulation of PSF2, a member of the GINS multiprotein complex, in intrahepatic cholangiocarcinoma. Oncol Rep 2005;14:701–6.
16. Hayashi R, Arauchi T, Tategu M, Goto Y, Yoshida K. A combined computational and experimental study on the structure-regulation relationships of putative mammalian DNA replication initiator GINS. Genomics Proteomics Bioinformatics 2006;4:156–64.
17. Ryu B, Kim DS, Deluca AM, Alani RM. Comprehensive expression profiling of tumor cell lines identifies molecular signatures of melanoma progression. PLoS One 2007;2:e594.
18. Ben-Porath I, Thomson MW, Carey VJ, et al. An embryonic stem cell-like gene expression signature in poorly differentiated aggressive human tumors. Nat Genet 2008;40:499–507.
19. Satoh N, Yamada Y, Kinugasa Y, Takakura N. Angiopoietin-1 alters tumor growth by stabilizing blood vessels or by promoting angiogenesis. Cancer Sci 2008;99:2373–9.
20. Kanda T, Sullivan KF, Wahl GM. Histone-GFP fusion protein enables sensitive analysis of chromosome dynamics in living mammalian cells. Curr Biol 1998;8:377–85.
21. Fujita H, Fukuhara S, Sakurai A, et al. Local activation of Rap1 contributes to directional vascular endothelial cell migration accompanied by extension of microtubules on which RAPL, a Rap1-associating molecule, localizes. J Biol Chem 2005;280:5022–31.
22. Fukuhara S, Sako K, Minami T, et al. Differential function of Tie2 at cell-cell contacts and cell-substratum contacts regulated by angiopoietin-1. Nat Cell Biol 2008;10:513–26.
23. Subramanian A, Tamayo P, Mootha VK, et al. Gene set enrichment analysis: a knowledge-based approach for interpreting genome-wide expression profiles. Proc Natl Acad Sci U S A 2005;102:15545–50.
24. Wong DJ, Liu H, Ridky TW, Cassarino D, Segal E, Chang HY. Module map of stem cell genes guides creation of epithelial cancer stem cells. Cell Stem Cell 2008;2:333–44.
25. Somervaille TC, Matheny CJ, Spencer GJ, et al. Hierarchical maintenance of MLL myeloid leukemia stem cells employs a transcriptional program shared with embryonic rather than adult stem cells. Cell Stem Cell 2009;4:129–40.
26. Calabrese C, Poppleton H, Kocak M, et al. A perivascular niche for brain tumor stem cells. Cancer Cell 2007;11:69–82.
27. Kiel MJ, Yilmaz OH, Iwashita T, Terhorst C, Morrison SJ. SLAM family receptors distinguish hematopoietic stem and progenitor cells and reveal endothelial niches for stem cells. Cell 2005;121:1109–21.
28. Tozer GM, Kanthou C, Baguley BC. Disrupting tumour blood vessels. Nat Rev Cancer 2005;5:423–35.
29. Paez-Ribes M, Allen E, Hudock J, et al. Antiangiogenic therapy elicits malignant progression of tumors to increased local invasion and distant metastasis. Cancer Cell 2009;15:220–31.
30. Okamoto R, Ueno M, Yamada Y, et al. Hematopoietic cells regulate the angiogenic switch during tumorigenesis. Blood 2005;105: 2757–63.
31. Kearsey SE, Cotterill S. Enigmatic variations: divergent modes of regulating eukaryotic DNA replication. Mol Cell 2003;12:1067–75.
32. Hemerly AS, Prasanth SG, Siddiqui K, Stillman B. Orc1 controls centriole and centrosome copy number in human cells. Science 2009; 323:789–93.
33. Prasanth SG, Prasanth KV, Stillman B. Orc6 involved in DNA replication, chromosome segregation, and cytokinesis. Science 2002;297: 1026–31.

Published OnlineFirst January 10, 2011; DOI:10.1158/1078-0432.CCR-10-1993

Clinical Cancer Research

Transient PI3K Inhibition Induces Apoptosis and Overcomes HGF-Mediated Resistance to EGFR-TKIs in *EGFR* Mutant Lung Cancer

Ivan S. Donev, Wei Wang, Tadaaki Yamada, et al.

Clin Cancer Res 2011;17:2260-2269. Published OnlineFirst January 10, 2011.

Published OnlineFirst January 10, 2011; DOI:10.1158/1078-0432.CCR-10-1993

Clinical Cancer Research

Transient PI3K Inhibition Induces Apoptosis and Overcomes HGF-Mediated Resistance to EGFR-TKIs in *EGFR* Mutant Lung Cancer

Ivan S. Donev[1], Wei Wang[1], Tadaaki Yamada[1], Qi Li[1], Shinji Takeuchi[1], Kunio Matsumoto[2], Takao Yamori[3], Yasuhiko Nishioka[4], Saburo Sone[4], and Seiji Yano[1]

Abstract

Purpose: Epidermal growth factor receptor (EGFR) tyrosine kinase inhibitors (TKI), such as gefitinib and erlotinib, show favorable response to *EGFR* mutant lung cancer. However, the responders acquire resistance almost without exception. We recently reported that hepatocyte growth factor (HGF) induces EGFR-TKI resistance by activating MET that restores downstream mitogen activated protein kinase (MAPK)/extracellular signal regulated kinase (ERK)1/2 and phosphoinositide 3-kinase (PI3K)/Akt signaling. The purpose of this study was to determine whether inhibition of PI3K, a downstream molecule of both EGFR and MET, could overcome HGF-mediated EGFR-TKI resistance in *EGFR* mutant lung cancer cells PC-9 and HCC827.

Experimental Design: We explored therapeutic effect of a class I PI3K inhibitor PI-103 on HGF-induced EGFR-TKI resistance *in vitro* and *in vivo*.

Results: Unlike gefitinib or erlotinib, continuous exposure with PI-103 inhibited proliferation of PC-9 and HCC827 cells, even in the presence of HGF. On the other hand, in gefitinib-resistant xenograft model by using PC-9 cells mixed with HGF high producing fibroblasts, PI-103 monotherapy did not inhibit tumor growth. However, PI-103 combined with gefitinib successfully regressed gefitinib-resistant tumor. *In vitro* experiments by considering short half-life of PI-103 reveal that transient exposure of PI-103 combined with gefitinib caused sustained inhibition of Akt phosphorylation, but not ERK1/2 phosphorylation, resulting in induction of tumor cell apoptosis even in the presence of HGF.

Conclusions: These results indicate that transient blockade of PI3K/Akt pathway by PI-103 and gefitinib could overcome HGF-mediated resistance to EGFR-TKIs by inducing apoptosis in *EGFR* mutant lung cancer. *Clin Cancer Res; 17(8); 2260–9. ©2011 AACR.*

Introduction

Lung cancer is one of the most prevalent malignancies and the leading cause of cancer-related death worldwide. Non–small cell lung cancer (NSCLC) accounts for nearly 80% of lung cancer cases. Substantial efforts are being made to identify the optimal target for NSCLC therapy. The tyrosine kinase inhibitors (TKI), such as gefitinib and erlotinib, have been shown to inhibit epidermal growth factor receptor (EGFR)-mediated downstream pathways, including mitogen activated protein kinase (MAPK)/extracellular signal regulated kinase (ERK)1/2 and phosphoinositide 3-kinase (PI3K)/Akt, and to show favorable activity in NSCLC patients with mutant *EGFR* (1). Recent phase III clinical trials showed that patients with *EGFR* mutant NSCLC had superior outcomes with gefitinib treatment, compared with standard first-line cytotoxic chemotherapy (2–3). However, the patients develop acquired resistance to EGFR-TKIs almost without exceptions within a couple of years (4). In addition, 20% to 25% patients with *EGFR* activating mutations show intrinsic resistance to EGFR-TKIs.

Two genetically conferred mechanisms–T790M second mutation in *EGFR* (4–5) and the *MET* gene amplification (6)—have been well reported to induce the acquired resistance to EGFR-TKIs in *EGFR* mutant lung cancer. Recently, we identified a third mechanism, hepatocyte growth factor (HGF)-induced resistance. It induces EGFR-TKI resistance by activating MET that restores phosphorylation of downstream MAPK/ERK1/2 and PI3K/Akt pathways (7–8). This is not a genetically conferred mechanism and may be involved in both intrinsic resistance and acquired resistance to EGFR-TKIs in *EGFR* mutant lung cancer (7). Although HGF is reported to be produced predominantly

Authors' Affiliations: [1]Division of Medical Oncology; [2]Division of Tumor Dynamics and Regulation, Cancer Research Institute, Kanazawa University, Kanazawa; [3]Division of Molecular Pharmacology, Cancer Chemotherapy Center, Japanese Foundation for Cancer Research, Tokyo; [4]Department of Respiratory Medicine & Rheumatology, Institute of Health Biosciences, University of Tokushima Graduate School, Tokushima, Japan

Note: Supplementary data for this article are available at Clinical Cancer Research Online (http://clincancerres.aacrjournals.org/).

Corresponding Author: Seiji Yano, Division of Medical Oncology, Cancer Research Institute, Kanazawa University, Kanazawa, Ishikawa 920-0934, Japan. Phone: +81-76-265-2780; Fax: +81-76-234-4524. E-mail: syano@staff.kanazawa-u.ac.jp

doi: 10.1158/1078-0432.CCR-10-1993

Published OnlineFirst January 10, 2011; DOI:10.1158/1078-0432.CCR-10-1993

Translational Relevance

The acquired resistance to epidermal growth factor receptor (EGFR) tyrosine kinase inhibitors (TKI) is one of the most serious problems on the management of *EGFR* mutant lung cancer. We recently reported the novel mechanism that hepatocyte growth factor (HGF) induces EGFR-TKI resistance by activating MET that restores phosphorylation of downstream mitogen activated protein kinase (MAPK)/extracellular signal regulated kinase (ERK)1/2 and phosphoinositide 3-kinase (PI3K)/Akt pathways.

In this study, we showed that transient blockade of PI3K/Akt pathway by PI3K inhibitor and gefitinib could overcome HGF-mediated resistance to EGFR-TKIs by inducing apoptosis in both *in vitro* and *in vivo* models. Our findings indicate usefulness of double blockade of EGFR and PI3K, and further postulate the need to develop PI3K inhibitor analogues with more suitable pharamcokinetics and metabolic profiles for more successful therapy of *EGFR* mutant lung cancer.

by stromal cells, it can act both autocrine and paracrine fashion when inducing resistance to EGFR-TKIs (7, 9). More recent studies showed that HGF is frequently coexpressed along with the T790M second mutation in *EGFR* (10) and *MET* gene amplification (8) in tumors of patients with acquired resistance to EGFR-TKIs, indicating the importance of HGF as therapeutic target for overcoming resistance to EGFR-TKIs.

Several strategies are available to block HGF-MET–mediated signaling, including ligand (HGF) blockade, MET tyrosine kinase inhibition, and inhibition of downstream molecules (PI3K/Akt, MAPK/ERK; ref. 11). PI3Ks are responsible for the generation of 3-phosphorylated inositides, including the important second messenger PtIns(3,4,5)P3 (antiphosphatidylinositol 3,4,5-triphosphate), resulting in activation of signal transduction pathways in many physiologic process (12). PI3Ks are divided into 3 classes on the basis of their primary structures and *in vitro* substrate specificity (13), with class I PI3Ks being the most well characterized. Class I PI3Ks can be further subdivided into class IA (p110α, p110β, and p110δ) and class IB (p110γ) according to their structure and interaction with p85 and p55 regulatory subunits. Class IA PI3Ks, each composed of a p85 regulatory subunit and a p110 catalytic subunit, are the most widely involved in cancer (14). The major effector of PI3K in cancer is Akt, a serine–threonin kinase that is directly activated in response to PI3K (13–14). Recent studies indicate that the PI3K/Akt pathway plays crucial roles in resistance to various types of TKIs, including EGFR TKIs (6, 15–17). Accordingly, a large numbers of PI3K inhibitors are being developed (18).

We sought to determine whether inhibition of PI3K signaling pathway could overcome EGFR-TKI resistance induced by HGF in *EGFR* mutant lung cancer. We found that transient exposure of class I PI3K inhibitor plus gefitinib was sufficient to overcome HGF-mediated resistance by inducing apoptosis of *EGFR* mutant lung cancer cells.

Materials and Methods

Cell cultures and reagents

The *EGFR* mutant human lung adenocarcinoma cell lines, with exon 19 deletion in *EGFR* PC-9 (del E746_A750) and HCC827 (del E746_A750), were purchased from Immuno-Biological Laboratories Co. and American Type Culture Collection, respectively (19). The H1975 human lung adenocarcinoma cell line with EGFR-L858R/T790M double mutation (20) was kindly provided by Dr. J.D. Minna (University of Texas Southwestern Medical Center, Dallas, TX) and Dr. Y. Sekido (Aichi Cancer Center Research Institute, Nagoya, Japan). Human lung embryonic fibroblasts, MRC-5, were obtained from RIKEN Cell Bank. The PC-9, HCC827, and H1975 cell lines were maintained in RPMI 1640 medium supplemented with 10% FBS and antibiotics. The MRC-5 (p30–p35) was cultured in 10% FBS DMEM (Dulbecco's modied Eagle's medium). All cells were passaged for less than 3 months before renewal from frozen, early-passage stocks obtained from the indicated sources. Cells were regularly screened for mycoplasma with the use of a MycoAlert Mycoplasma Detection Kit (Lonza). Gefitinib, erlotinib, PI-103 (PI3K α inhibitor 1), and GDC-0941 were obtained from AstraZeneca, Chugai Pharmaceutical Co., Calbiochem, and Selleck Chemicals, respectively. Human recombinant HGF was prepared as described previously (21).

Cell proliferation assay

Cell proliferation was measured by the MTT dye reduction method (22). Tumor cells (2×10^3/100 μL per well) were plated into each well of 96-well plates in RPMI 1640 with 10% FBS. After 24 hours incubation, several concentrations of gefitinib, erlotinib, PI-103, and/or HGF were added to each well, and incubation was continued for a further 72 or 48 hours. For short exposure to gefitinib and/or PI-103, tumor cells (8×10^3/800 μL per well) were incubated in 24-well plates. After 24 hours incubation, several concentrations of PI-103 and gefitinib were added for 1 hour, then washed 2 times with PBS, and then replated with fresh medium. Viability was assessed at 48 hours after initial exposure. Cell proliferation was determined with MTT solution (2 mg/mL; Sigma) as described previously (7). Each experiment was done at least 3 times, each with triplicate samples.

Determination of drug synergy

Cells were seeded at a density of 2×10^3 per well of a 96-well plate. Concentration ranges were chosen to span the complete dose-response range of both drugs. All treatments were done in quadruplicate. Cell proliferation/viability was determined after 3 days by using MTT assay. Multiple drug effect analysis was done by using CalcuSyn Software (Biosoft), which quantitatively describes the interaction

Published OnlineFirst January 10, 2011; DOI:10.1158/1078-0432.CCR-10-1993

between 2 or more drugs (23). This method assigns combination index (CI) values to each drug combination and defines drug synergy when a CI value is less than 1 or drug antagonism when a CI value is greater than 1.

Coculture of lung cancer cells with fibroblasts

Cells were cocultured in transwell chambers separated by 8 μm pore filters. Tumor cells (8×10^3 cells/700 μL) with gefitinib and or PI-103 different doses were placed in the bottom chamber, and fibroblasts (10^4 cells/300 μL) were placed in the top chamber. After 72 hours, the top chamber was removed and cell proliferation was measured by MTT assay. For short exposure to PI-103 and/or gefitinib, the proliferation was assessed after 48 hours and drugs were administered for only 1 hour in different concentration, and then each well was washed twice with PBS and new fresh media were added. Each experiment was done at least 3 times, each with triplicate samples.

Assay for RNA interference

Duplexed Stealth RNAi (Invitrogen) against Akt1-1 (5′-AUACCGGCAAAGAAGCGAUGCUGCA-3′), Akt1-2 (5′-AACCCUCCUUCACAAUAGCCACGUC-3′), and Akt1-3 (5′-UAGCGUGGCCGCCAGGUCUUGAUGU-3′) was used for RNA interference assay. One day before transfection, aliquots of 2×10^4 tumor cells in 400 μL of antibiotic-free medium were plated on 24-well plates. After incubation for 24 hours, the cells were transfected with siRNA (50 pmol) or scramble RNA by using Lipofectamine 2000 (1 μL) in accordance with the manufacturer's instructions. After 24 hours incubation, the cells were washed with PBS and incubated with or without gefitinib (0.1 μmol/L) and/or rhHGF (recombinant human HGF, 20 ng/mL) for an additional 72 hours in antibiotic-containing medium. Cell proliferation was measured by a Cell Counting Kit-8 (Dojin) in accordance with the manufacturer's instructions. Each experiment was done at least in triplicate and 3 times independently.

Xenograft studies in SCID mice

Suspensions of PC-9 cells (5×10^6) with MRC-5 (5×10^6) were injected subcutaneously into the backs of 5-week-old female severe combined immunodeficient mice (SCID). Mice ($n = 6$ per group) were randomized to: (a) control group, (b) gefitinib only (25 mg/kg/d) orally, (c) PI-103 only prepared in 20% 4-hydroxypropyl β-cyclodextrin (5 mg/kg/d) intraperitoneally, or (d) gefitinib (25 mg/kg/d) and PI-103 (5 mg/kg/d). After 4 days (tumors diameter >4 mm), the treatment was started. The tumor volume was calculated ($mm^3 = width^2 \times length/2$). All animal experiments complied with the guidelines for the Institute for Experimental Animals, Advanced Science Research Center, Kanazawa University, Kanazawa, Japan (approval no. AP-081088).

Antibodies and Western blotting

For Western blotting analysis, 40 μg of total protein were resolved by SDS polyacrylamide gel (Bio-Rad) electrophoresis and the proteins were then transferred onto polyvinylidene difluoride membranes (Bio-Rad). After washing 4 times, membranes were incubated with Blocking One (Nacalai Tesque, Inc.) for 1 hour at room temperature and then incubated overnight at 4°C with the following primary antibodies: anti-MET (25H2), anti-phospho-MET (anti-p-MET, Y1234/Y1235; 3D7), anti-p-EGFR (Y1068), anti-ErbB3 (1B2), anti-p-ErbB3 (Tyr1289; 21D3), anti-Akt or p-Akt (Ser473), anti-cleaved caspase-9 (Asp315), anti-cleaved caspase-3 (Asp175), anti-cleaved PARP (Asp214) antibodies (1:1,000 dilution, Cell Signaling Technology), anti-human EGFR (1 μg/mL), anti-human/mouse/rat ERK-1/ERK-2 (0.2 μg/mL), or anti-p-ERK-1/ERK-2 (T202/Y204; 0.1 μg/mL) antibodies (R&D Systems). After washing thrice, membranes were incubated for 1 hour at room temperature with species-specific horseradish peroxidase–conjugated secondary antibodies. Immunoreactive bands were visualized with SuperSignal West Dura Extended Duration Substrate, an enhanced chemiluminescent substrate (Pierce Biotechnology). Each experiment was done at least thrice independently.

TUNEL assay

Terminal deoxynucleotidyl transferase–mediated nick end labeling staining was performed by the Apoptosis Detection System (Promega). Briefly, the frozen tissue sections (9 μm thick) were fixed with PBS containing 4% formalin. The slides were washed with PBS and permeabilized with 0.2% Triton X-100. The samples were then equilibrated, and DNA strand breaks were labeled with fluorescein-12-dUTP (fluorescein-12-2-deoxy-uridine-5-triphosphate) by adding nucleotide mixture and terminal deoxynucleotidyl transferase enzyme. The reaction was stopped with saline sodium citrate, and the localized green fluorescence of apoptotic cells was detected by fluorescence microscopy (×200).

Reverse transcriptase-PCR analysis

Total RNA was isolated from MRC-5 cells treated with various concentration of PI-103 for 24 hours, with ISOGEN RNA extraction. Total RNAs were reversely transcribed by an Omniscript RT Kit (Qiagen) according to the manufacturer's protocols. The primers for HGF and β-actin were as follow: HGF forward, 5′-CAGTGTTGAGAAGTTGAATGC-3′, reverse, 5′-GTGTCATTCATAGTATTGTGAG-3′, and β-actin forward, 5′-AAGAGAGGCATCCTCACCCT-3′, reverse, 5′-TACATGGCTGGGGTGTTGAA-3′. Polymerase chain reaction was done by Ex Taq Hot Start Version (Takara). Cycles for HGF and β-actin were 28 and 26, respectively. The bands were visualized by ethidium bromide staining.

Cell apoptosis assay

Cell apoptosis induced by gefitinib was detected with an Annexin V-FITC Apoptosis Detection Kit I (BD Biosciences Pharmingen) in accordance with the manufacturer's protocols as described previously (7). The analysis was done

Published OnlineFirst January 10, 2011; DOI:10.1158/1078-0432.CCR-10-1993

on a FACSCalibur flow cytometer with CellQuest Software (Becton Dickinson).

Statistical analysis

Two-tailed Student's *t* test was performed, when noted, by GraphPad Software. Differences of $P < 0.001$ were considered statistically different (24).

Results

Continuous exposure of PI-103 effectively suppresses the *in vitro* proliferation of EGFR mutant lung cancer cells in the presence of HGF

Both PC-9 and HCC827 cells were highly sensitive to continuous exposure (72 hours) to gefitinib and erlotinib. HGF alone did not affect proliferation of PC-9 cells, but it slightly stimulated the proliferation of HCC827 cells. Under these experimental conditions, HGF dose dependently induced resistance to gefitinib and erlotinib of PC-9 and HCC827 cells (Fig. 1), as reported previously (7). Under the same experimental conditions, continuous exposure (72 hours) of PI-103 inhibited the proliferation of PC-9 and HCC827 cells though the IC_{50} (half maximal inhibitory concentration) to PI-103 was higher (0.3 μmol/L for HCC827; 0.8 μmol/L for PC-9 cells) than gefitinib (0.01 μmol/L for HCC827; 0.03 μmol/L for PC-9 cells) and erlotinib (0.01 μmol/L for HCC827; 0.02 μmol/L for PC-9 cells). Importantly, HGF did not decrease the sensitivity of PC-9 and HCC827 cells to PI-103, suggesting the potential of PI-103 to overcome HGF-induced resistance to gefitinib and erlotinib *in vitro*.

We recently reported that HGF induces resistance in lung cancer cells (H1975) with *EGFR* T790M second mutation to irreversible EGFR-TKI that is expected to overcome T790M second-mutation–mediated resistance to gefitinib or erlotinib (25). Interestingly, continuous exposure (72 hours) of PI-103 inhibited proliferation of H1975 cells in a dose-dependent manner (Supplementary Fig. S1). HGF slightly stimulated proliferation of H1975 cells and induced the resistance to irreversible EGFR-TKI, CL-387,785 (N-[4-[(3-bromophenyl)amino]-6-quinazolinyl]-2-butynamide). However, HGF did not affect the sensitivity of H1975 cells to PI-103. These results suggest that PI-103 has potential to overcome HGF-induced resistance to not only reversible EGFR-TKIs but also irreversible EGFR TKIs. Moreover, combined use of PI-103 with CL-387,785 further inhibited proliferation of H1975 cells, irrespective of the presence of HGF.

We next examined whether PI-103 sensitized *EGFR* mutant lung cancer cells when combined with gefitinib in the presence or absence of HGF. PI-103 inhibited the proliferation of PC-9 and HCC827 cells in a dose-dependent manner. Gefitinib markedly suppressed the proliferation, and HGF induced the resistance to gefitinib. Surprisingly, PI-103 combined with gefitinib further inhibited the proliferation of PC-9 and HCC827 cells not only in the absence of HGF but also in the presence of HGF (Fig. 2A). Proliferation data were analyzed by the established method of Chou and Talalay (23) by using CalcuSyn software. The resulting CI values were les than 1 over most of the effect range of the drugs, demonstrating that the combination of PI-103 and gefitinib inhibited the proliferation synergistically in PC-9 and HCC827 cells. Same results were reproduced with GDC-0941–a derivative of PI103 with improved pharmacokinetic and pharmacodynamic properties that are active against all isoforms of class

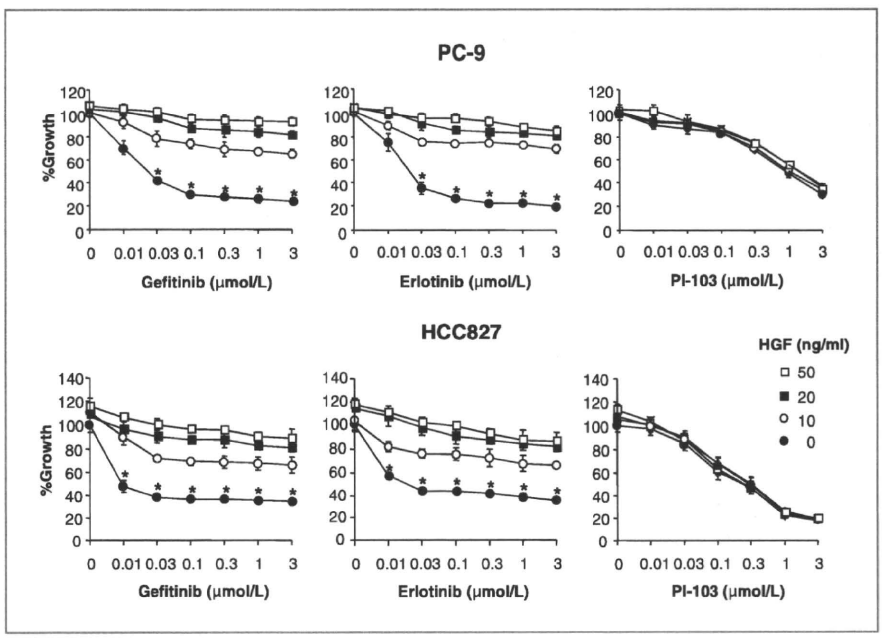

Figure 1. Continuous exposure of PI-103 suppresses the *in vitro* proliferation of *EGFR* mutant lung cancer cells, irrespective of the presence of HGF. Tumor cells were continuously treated with increasing concentrations of EGFR-TKI (gefitinib or erlotinib) or PI-103, with or without HGF, and cell growth was determined after 72 hours by MTT assay. Data shown are the representative of 5 independent experiments. Error bars indicate SD of triplicate cultures. *, $P < 0.001$ (Student's *t* test).

Published OnlineFirst January 10, 2011; DOI:10.1158/1078-0432.CCR-10-1993

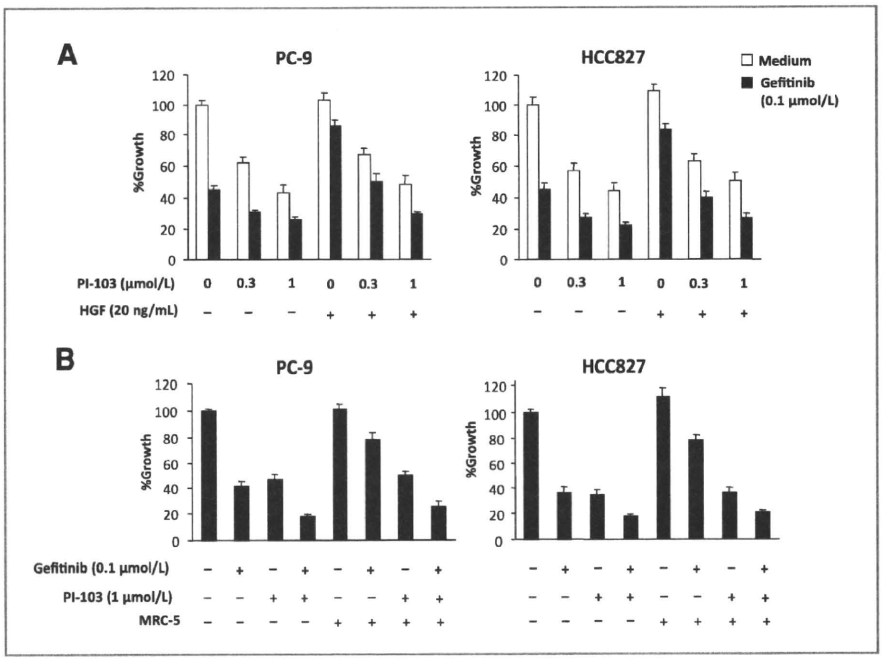

Figure 2. PI-103 combined with gefitinib overcomes HGF-induced gefitinib resistance *in vitro*. A, tumor cells were continuously treated with various concentrations of gefitinib and PI-103, with or without HGF, and cell growth was determined after 48 hours by MTT assay. B, tumor cells were cocultured with human lung fibroblasts (MRC-5) and were continuously treated with indicated concentrations of gefitinib, and/or PI-103. Cell growth was determined after 48 hours by MTT assay. Data shown are the representative of 3 independent experiments. Error bars indicate SD of triplicate cultures.

I PI3Ks and now used in clinical trials in patients with solid tumors (26; Supplementary Fig. 2). This synergy was also observed in a coculture system where HGF high producing fibroblasts, MRC-5, induced gefitinib resistance. While PI-103 did not inhibit HGF expression in MRC-5 cells (Supplementary Fig. S3), PI-103 synergistically inhibited the proliferation of PC-9 and HCC827 cells, irrespective of the presence of MRC-5 cells, when combined with gefitinib (Fig. 2B). These results suggest that PI3K inhibitor combined with gefitinib may be more beneficial than either monotherapy.

PI-103 with or without gefitinib suppresses PI3K/Akt pathway even in the presence of HGF

To explore the molecular mechanism by which PI-103 combined with gefitinib showed greater antiproliferative effect, we examined the phosphorylation of MET, EGFR, ErbB3, and their downstream pathways (PI3K/Akt and ERK1/2) by Western blotting (Fig. 3A). PC-9 and HCC827 cells expressed EGFR, ErbB3, and MET proteins, and these molecules were phosphorylated at various levels. These receptors and downstream molecules, such as Akt and ERK1/2, were also phosphorylated. While HGF alone did not affect phosphorylation of EGFR or ErbB3, it stimulated phosphorylation of MET and thereby activated Akt and ERK1/2. Although gefitinib inhibited phosphorylation of Akt and ERK1/2 in the absence of HGF, it failed to inhibited Akt and ERK1/2 phosphorylation in the presence of HGF. Importantly, PI-103 did not affect the phosphorylation of ERK1/2 or upstream molecules such as MET, EGFR, and ErbB3, but did inhibit the phosphotylation of Akt, regardless of presence of HGF. In addition, PI-103 combined with gefitinib inhibited phosphorylation of both Akt and ERK1/2 in the absence of HGF. The combination of PI-103 and gefitinib inhibited Akt phosphorylation, even in the presence of HGF, but failed to inhibit ERK1/2 phosphorylation. These results confirm our previous observations (7) and further suggest that PI-103 overcomes this resistance by inhibiting phosphorylation of downstream PI3K/Akt. The importance of PI3K/Akt as a target of PI-103 was further supported the evidence obtained in experiments with siRNA for Akt. Treatment with siAkt1 alone knocked down the Akt expression in PC-9 cells (Fig. 3B) and resulted in inhibition of cell proliferation by 20% (Fig. 3C). Notably, the treatment with siAkt1 reversed HGF-induced gefitinib resistance in combination with gefitinib (Fig. 3C).

PI-103 combined with gefitinib overcomes HGF-induced gefitinib resistance *in vivo*

We recently established an *in vivo* model by inoculating PC-9 cells premixed with HGF high producing MRC-5 cells and showed that gefitinib resistance that was abrogated by HGF-MET inhibition (9). By using this model, we next evaluated whether PI-103 overcomes HGF-induced resistance to gefitinib *in vivo*. Consistent with previous observations, we found that treatment with gefitinib alone prevented the enlargement of tumors produced by the mixture of PC-9 cells and MRC-5 cells, but did not cause tumor regression. Since gefitinib induces tumor shrinkage of PC-9 tumors (9), our results suggest that MRC-5 cells induced gefitinib resistance *in vivo*. Under these experimental conditions, treatment with PI-103 alone did not inhibit tumor growth, whereas combined treatment with PI-103 and gefitinib dramati-

Published OnlineFirst January 10, 2011; DOI:10.1158/1078-0432.CCR-10-1993

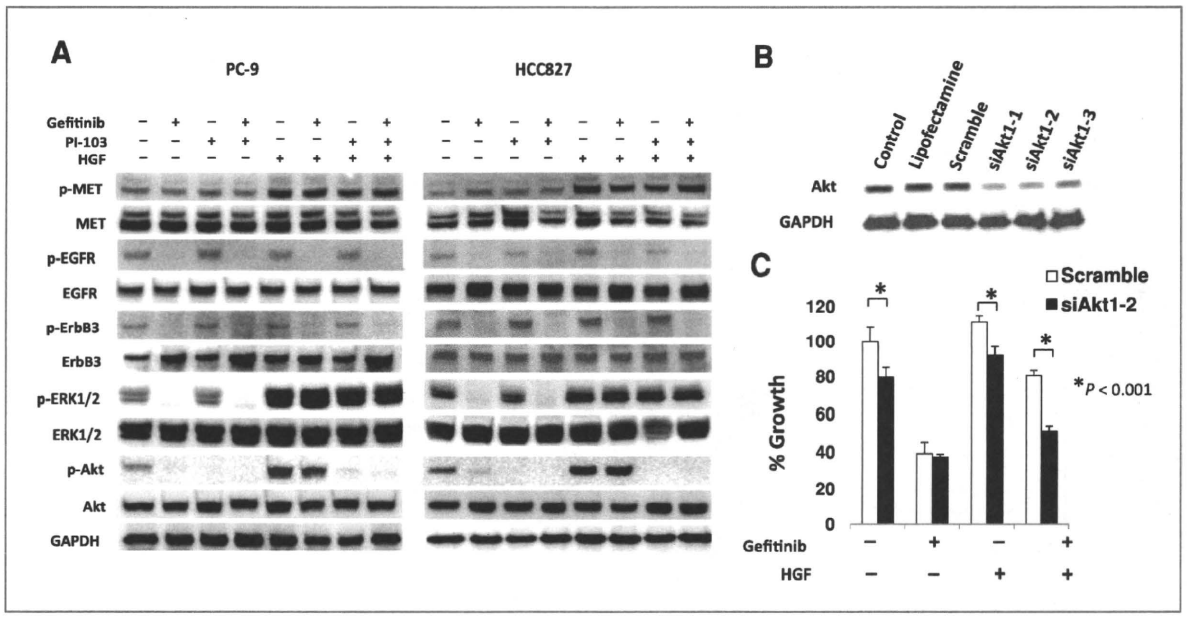

Figure 3. PI-103 with or without gefitinib suppresses PI3K/Akt pathway even in the presence of HGF. A, tumor cells were treated with or without gefitinib (1 μmol/L), PI-103 (1 μmol/L), and/or HGF (20 ng/mL) for 1 hour. Then, cells were lyzed, and the indicated proteins were detected by immunoblotting. Data shown are the representative of 3 independent experiments. B, PC-9 cells were treated with 3 different siRNAs specific for Akt1 or scramble siRNA. C, resultant cells were treated with gefitinib (0.1 μmol/L) and or HGF (20 ng/mL) for 48 hours. Then, MTT assay was performed. GAPDH, glyceraldehyde 3-phosphate dehydrogenase.

cally regressed the tumors (Fig. 4A and B). Similar results were reproduced by GDC-0941 that is now used in clinical trials in patients with solid tumors (Supplementary Fig. S4). These combined treatments did not cause obvious side effects, such as weight loss of the mice.

We further examined apoptotic cells in the tumors treated with gefitinib and/or PI-103. Although there were few apoptotic cells in control-treated (Fig. 4C) or PI-103–treated tumors (Fig. 4D), discernible numbers of apoptotic cells were detected in gefitinib-treated tumors (Fig. 4E). However, more apoptotic cells were found in tumors treated with both PI-103 and gefitinib (Fig. 4F; Fig. 4A and B). Immunoblots with these tumors revealed that treatment with PI-103 with or without gefitinib did not affect the phosphorylation of ERK1/2. On the other hand, PI-103 alone or in combination with gefitinib inhibited Akt phosphorylation in the tumor. Most notably, PI-103 combined with gefitinib induced cleaved caspase-3, the effector caspase that mediates death signaling (Fig. 4G). These results strongly suggested the importance of PI3K/Akt as a target of this combined therapy.

Short exposure of PI-103 combined with gefitinib further inhibits Akt mediating signal and proliferation of EGFR mutant lung cancer cells

Our finding that PI-103 monotherapy did not inhibit tumor growth, whereas PI-103 overcame synergistically HGF (MRC-5)-induced gefitinib resistance when combined with gefitinib, was unexpected. Although PI-103 has been reported to have very rapid tissue distribution and tissue clearance *in vivo* (half-life of PI-103 in the major organs is 0.7–1.3 hours; ref. 12), we hypothesized that rapid tissue clearance of PI-103 might be responsible for its insufficient therapeutic effect *in vivo*. To mimic pharmacodynamics of PI-103 *in vivo*, we exposed PC-9 and HCC827 cells to PI-103 transiently for 1 hour, washed the cells, and incubated the resultant cultures in fresh medium for 48 hours (Fig. 5A). Transient exposure to PI-103 resulted only in approximately 15% inhibition of the proliferation of PC-9 or HCC827 cells, whereas transient exposure to gefitinib resulted in higher inhibition of proliferation (>30%). Importantly, transient exposure to both PI-103 and gefitinib inhibited the proliferation of these 2 cell lines, reaching IC_{50} (Fig. 5B). Analysis using CalcuSyn software (23) indicates that the effect was synergistic. These phenomena were also observed when *EGFR* mutant cancer cells were cocultured with MRC-5 cells (Fig. 5C) to induce gefitinib resistance, representing the therapeutic efficacy seen *in vivo* model. In contrast, transient exposure to PI-103 and/or gefitinib did not inhibit proliferation of MRC-5 cells (Fig. 5D).

We further evaluated the kinetics of PI3K/Akt phosphorylation after transient exposure of PC-9 cells to PI-103 and gefitinib (Fig. 6A). As shown earlier (Fig. 3), 1 hour treatment with either PI-103 or gefitinib completely inhibited Akt phosphorylation in the absence of HGF. We found out that in the absence of HGF, gefitinib, alone or combined with PI-103, inhibited Akt phosphorylation for up to

Published OnlineFirst January 10, 2011; DOI:10.1158/1078-0432.CCR-10-1993

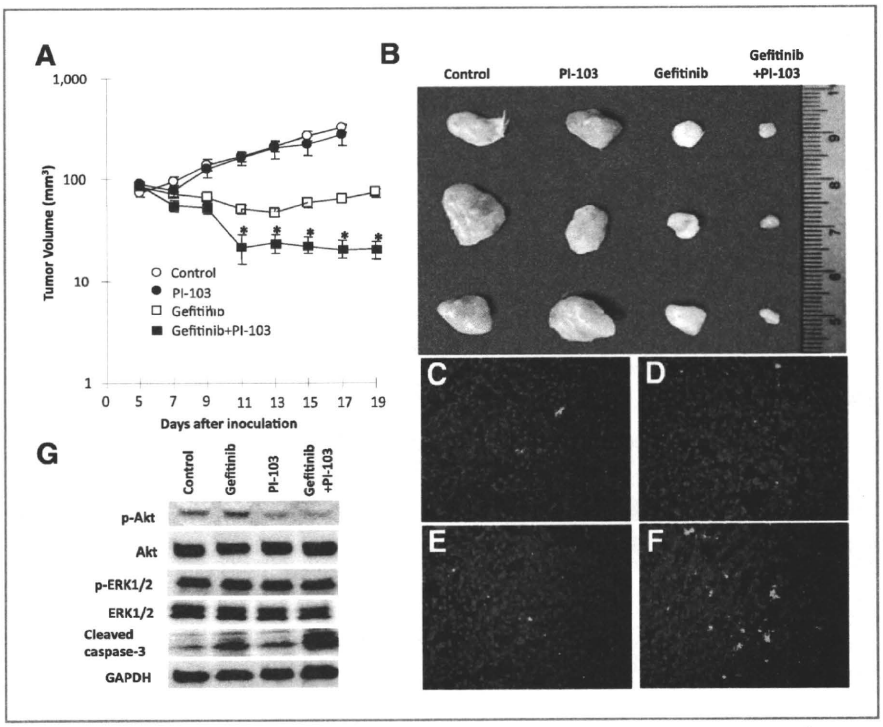

Figure 4. PI-103 combined with gefitinib overcomes HGF-induced gefitinib resistance *in vivo*. A, PC-9 cells (5×10^6) mixed with MRC-5 cells (5×10^6) were inoculated subcutaneously into SCID mice on day 0. Mice received oral gefitinib (25 mg/kg/d) and/or intraperitoneal PI-103 (5 mg/kg/d), starting on day 4. The tumor size was measured every 2 days and tumor volumes were calculated as described in Materials and Methods. Data shown are the representative of 2 independent experiments. Error bars indicate standard errors of 6 mice. *, $P < 0.001$ (Student's t test). B, macroscopic appearances of representative tumors harvested on day 19 are shown. Apoptotic cells were stained by TUNEL method as described in Materials and Methods. C, control. D, PI-103 alone. E, gefitinib alone. F, gefitinib + PI-103. G, tumors were harvested 1 hour after treatment on day 6. Tumor lysates were analyzed by immunoblotting with the indicated antibodies.

1 hour; subsequently, however, Akt phosphorylation in PC-9 cells treated with PI-103 alone started to recover. In the presence of HGF, gefitinib did not inhibit Akt phosphorylation, whereas Akt phosphorylation in PC-9 cells treated with PI-103 alone recovered by 1 hour after washing. However, cells treated with PI-103 plus gefitinib showed inhibition of Akt phosphorylation 1 hour after washing (Fig. 6A). More importantly, transient exposure to PI-103 plus gefitinib, but not either alone, resulted in the induction of cleaved caspase-9 and caspase-3, the initiator and effector caspases that mediate death signaling and cleaved PARP (Fig. 6A). Flow cytometry analyses with Annexin V further confirmed that transient exposure with PI-103 plus gefitinib induced apoptosis of HGF-treated PC-9 cells (Fig. 6B). These findings indicate that transient exposure to PI-103 combined with gefitinib is sufficient for inducing death signaling even in the presence of HGF, supporting the results observed *in vivo* experiments.

Discussion

Accumulating evidence indicate that HGF-MET axis is considerable therapeutic target for several solid tumors. HGF can act as autocrine growth factors for glioblastoma, thyroid cancer, and gastric cancer. Moreover, HGF stimulates the invasion and dissemination of various types of cancers (27), and inducing EGFR-TKI resistance in *EGFR* mutant lung cancer. In contrast to *MET* amplification–induced resistance, restoring the PI3K/Akt pathway and mediated by ErbB3 as an adaptor, HGF activates normal MET receptor and induces the resistance that restores PI3K/Akt pathway mediated by Gab1/2 as an adaptor (7–8). HGF also accelerates the expansion of preexisting clones with MET gene amplification and facilitates the induction of EGFR-TKI resistance in a population of *EGFR* mutant lung cancer (8). In addition, HGF frequently detected in EGFR-TKI–resistant tumors with *EGFR*-T790M second mutation and may induce the resistance to irreversible EGFR-TKIs (25). These observations highlight an important role of HGF ligand in controlling of tumor progression and drug sensitivity.

We have shown here that the combination of gefitinib and class I PI3K inhibitors, PI-103 and GDC-0941, overcame HGF-mediated gefitinib resistance in *EGFR* mutant lung cancer cells. Although HGF restored ERK1/2 and PI3K/Akt phosphorylation via MET activation even in the presence of gefitinib, transient exposure of PI-103 plus gefitinib efficiently inhibited PI3K/Akt phosphorylation, induced death signaling, and caused apoptosis of PC-9 cells. The combined treatment with PI-103 and gefitinib did not inhibit phosphorylation of ERK1/2 (Fig. 3) or STAT3 (data not shown). Recently, it was shown that transient potent inhibition of BCR-ABL kinase activity is associated with maximal clinical benefit in patients with chronic myelogenous leukemia (CML; ref. 28). Our results illustrate the possibility that transient double blockade of EGFR and PI3K may be useful for controlling HGF-induced resistance to EGFR-TKIs in *EGFR* mutant lung cancer.

A large number of PI3K inhibitors are developed and are being evaluated in the preclinical and clinical trials (18,

Published OnlineFirst January 10, 2011; DOI:10.1158/1078-0432.CCR-10-1993

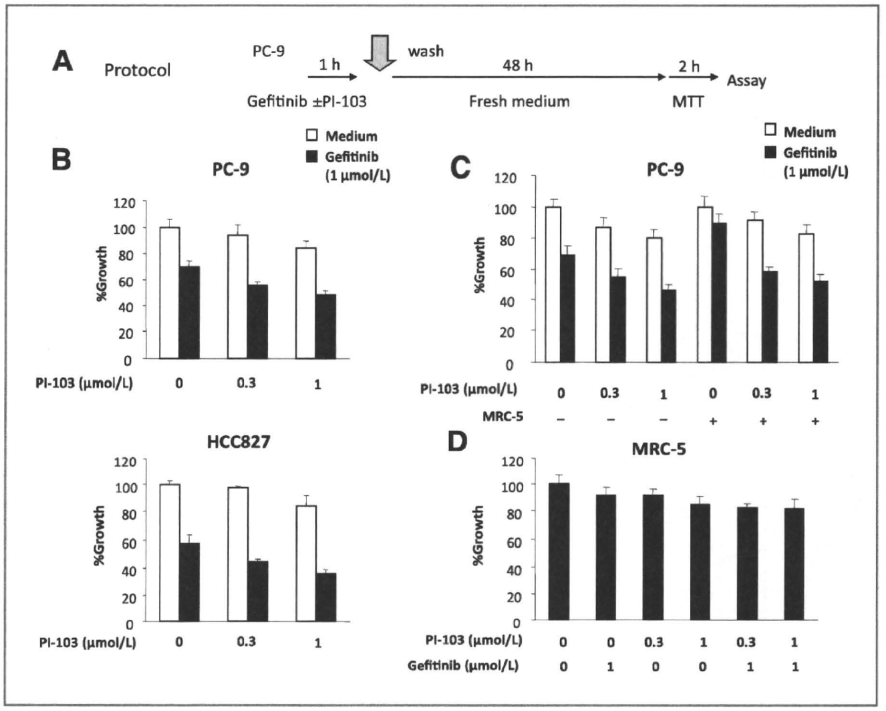

Figure 5. Short exposure of PI-103 combined with gefitinib effectively suppressed the proliferation of PC-9 and HCC827, but not MRC-5 cells. A, protocol. B, tumor cells were incubated with different concentrations of PI-103 and/or gefitinib for 1 hour, washed twice with PBS, and incubated in fresh medium for 48 hours. C, tumor cells were incubated with MRC-5 cells and different concentrations of PI-103 and/or gefitinib for 1 hour, washed twice with PBS, and coincubated with MRC-5 cells in fresh medium for 48 hours. D, MRC-5 cells were treated with different concentrations of PI-103 and/or gefitinib for 1 hour, washed twice with PBS, and further incubated in fresh medium for 48 hours. The cell growth was determined by MTT assay. Data shown are the representative of 3 independent experiments. Error bars indicate SD of triplicate cultures.

29). PI3K inhibitors have been found to induce G0/G1 cell arrest rather than apoptosis, and primarily causing stasis of tumor growth *in vivo* without substantial tumor shrinkage. For example, intraperitoneal administration of high doses of PI-103 (30–70 mg/kg) resulted in growth inhibition rather than regression in a range of human tumor xenografts (12, 30). Moreover, in *EGFR* mutant or *k-ras* mutant lung cancer models, tumor regression associating with apoptosis was observed only when PI3K/Akt pathway and MEK/MAPK pathway were simultaneously blocked (24, 31). Since these 2 pathways collaborate with each other to maintain cell survival, simultaneous blockade of both pathways is necessary to induce apoptosis. Surprisingly, our *in vitro* experiments revealed that though transient exposure of PI-103 plus gefitinib failed to inhibit ERK1/2 phosphorylation, it caused sustained PI3K/Akt inhibition, induced proapoptotic molecules, such as cleaved caspase-3 and caspase-9 and PARP, and thereby induced PC-9 cell apoptosis even in the presence of HGF. The mechanism by which combined use of PI-103 and gefitinib induces apoptosis of PC-9 cells, even in the presence of HGF, is not fully understood at present. One possible explanation is that double blockade of PI3K/Akt signaling pathway at upstream (EGFR level) and downstream (PI3K/Akt level) is efficient for inducing the apoptosis. The other possibility is that combined use of PI-103 and gefitinib inhibited the unknown pathway(s) that are responsible for survival of EGFR mutant lung cancer cells. While the combined therapy did not inhibit phosphorylation of STAT3 (data not shown) in PC-9 cells, we cannot rule out the involvement of other unknown pathway(s). Further experiments are warranted to clarify the mechanisms in future.

PI-103 is a class I PI3K inhibitor that reported favorable antitumor activity without any obvious side effects in preclinical animal models (12, 32). Pharmacokinetically, PI-103 is metabolized to form glucuronide and is cleared rapidly from plasma, with metabolysis of more than 70% PI-103 after 30 minutes of incubation with human and mouse microsomes (12). This is consistent with our results, showing that Akt phosphorylation in PC-9 cells treated with PI-103 alone was recovered by 1 hour (Fig. 6). PI-103 is not in clinical trials and work is now in progress to optimize its pharmacokinetics properties by structural modification (13). While continuous exposure for 72 hours of PI-103 inhibited the proliferation of PC-9 and HCC827 cells, transient exposure for 1 hour of PI-103 failed to do so *in vitro* condition. *In vivo* treatment with PI-103 (5 mg/kg intraperitoneally, once a day) also failed to inhibit the growth of PC-9 cells mixed with HGF high producing fibroblasts (MRC-5). Collectively, the insufficient effect of PI-103 monotherapy may be, at least in part, due to short half-life and rapid metabolism of this drug *in vivo*. GDC-0941 (5 mg/kg pharmacokinetics of oral, once a day) also failed to inhibit the growth of PC-9 cells mixed with MRC-5 cells. Though GDC-0941 is a derivative of PI103 with improved pharmacokinetic and pharmacodynamic properties, intratumoral concentration of GDC-0941 might not be enough to inhibit tumor growth in our *in vivo* experimental conditions. However, GDC-0941,

Published OnlineFirst January 10, 2011; DOI:10.1158/1078-0432.CCR-10-1993

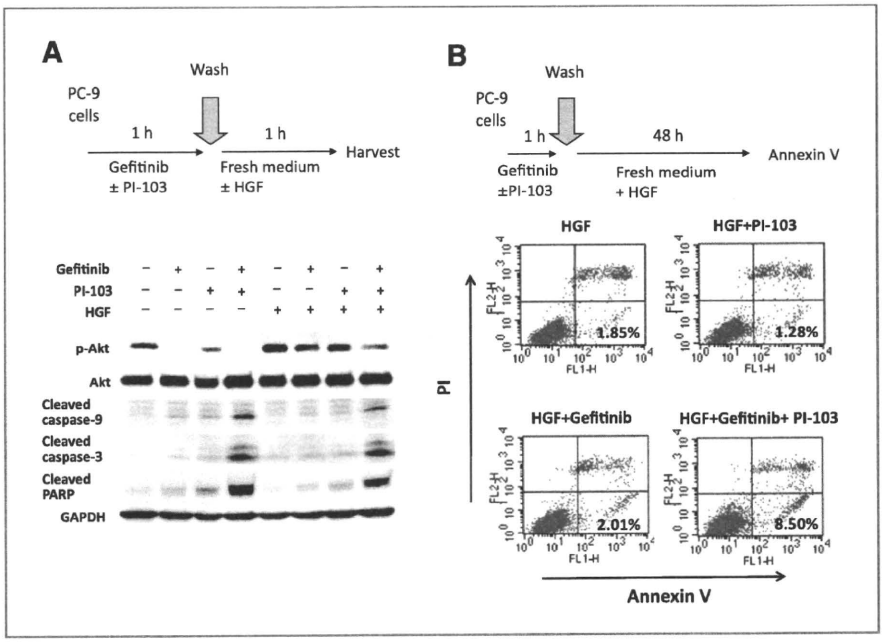

Figure 6. Apoptosis and time kinetics of phosphorylated Akt and proapoptotic molecules after short exposure to PI-103 and/or gefitinib. A, PC-9 cells were incubated (1 μmol/L), PI-103 (1 μmol/L), and/or HGF (20 ng/mL) for 1 hour. Then, the resultant cultures were incubated in fresh medium for 1 hour. Then, the cells were lyzed, and the indicated proteins were detected by immunoblotting. B, PC-9 cells were incubated with HGF (20 ng/mL) and PI-103 (1 μmol/L), and/or gefitinib (1 μmol/L), for 1 hour, and then washed 2 times with PBS. The resultant cultures were incubated in fresh medium for 24 hours. The apoptotic cells were determined by Annexin V assay kit according to manufactory protocol. Values shown are percentage of apoptotic cells. FL1-H and FL2-H, heights of fluorescence intensity.

like PI-103, successfully reversed the resistance when combined with gefitinib (Supplementary Fig. S4). Since we did not use maximum tolerated dose of these PI3K inhibitors (70–150 mg/kg; refs. 12, 26), our findings suggest that suboptimal dose of PI3K inhibitors may overcome HGF-induced resistance if combined with EGFR-TKIs.

In this study, we showed the possibility that double blockade of PI3K/Akt signaling pathway at upstream (EGFR level) and downstream (PI3K/Akt level) may be useful for overcoming HGF-induced resistance to EGFR-TKIs in *EGFR* mutant lung cancer cells. This concept can also be applicable to circumvent HGF-induced resistance to irreversible EGFR-TKIs (25). Moreover, cancer cell populations were recently shown to exhibit reversible tolerance to EGFR-TKIs by maintaining a phenotypical distinct subpopulation of cells that can protect the overall population from eradication by EGFR-TKIs (33). This reversible tolerance is mediated by activation of insulin like growth factor (IGF)-1 receptor (IGF-1R), but can be overcome by IGF-1R inhibitor combined with gefitinib ((35). Since PI3K/Akt is involved in IGF-1R–mediating signaling, the combined use of PI3K inhibitor may also protect against the emergence of reversibly tolerant subpopulations and may potently eradicate *EGFR* mutant lung cancer. Further investigations in PI3K/Akt signaling pathway are warranted for developing more successful compounds with better activity and safety for *EGFR* mutant lung cancer patients.

Disclosure of Potential Conflicts of Interest

No potential conflicts of interest were disclosed.

Acknowledgements

We thank Dr. J.D. Minna and Dr. Y. Sekido for kindly providing H1975 cells.

Grant Support

This study was supported by Grants-in-Aid of Cancer Research from the Ministry of Education, Science, Sports, and Culture of Japan (S. Yano, 21390256 and 22112010A01).

The costs of publication of this article were defrayed in part by the payment of page charges. This article must therefore be hereby marked *advertisement* in accordance with 18 U.S.C. Section 1734 solely to indicate this fact.

Received July 26, 2010; revised November 24, 2010; accepted December 18, 2010; published OnlineFirst January 10, 2011.

References

1. Pao W, Miller VA. Epidermal growth factor receptor mutations, small-molecule kinase inhibitors, and non-small-cell lung cancer: current knowledge and future directions. J Clin Oncol 2005;23:2556–68.
2. Mok TS, Wu YL, Thongprasert S, Yang CH, Chu DT, Saijo N, et al. Gefitinib or carboplatin-paclitaxel in pulmonary adenocarcinoma. N Engl J Med 2009;361:947–57.
3. Mitsudomi T, Morita S, Yatabe Y, Negoro S, Okamoto I, Tsurutani J, et al. Gefitinib versus cisplatin plus docetaxel in patients with non-small-cell lung cancer harbouring mutations of the epidermal growth factor receptor (WJTOG3405): an open label, randomised phase 3 trial. Lancet Oncol 2010;11:121–8.
4. Pao W, Miller VA, Politi KA, Riely GJ, Somwar R, Zakowski MF, et al. Acquired resistance of lung adenocarcinomas to gefitinib or erlotinib

Published OnlineFirst January 10, 2011; DOI:10.1158/1078-0432.CCR-10-1993

is associated with a second mutation in the EGFR kinase domain. PLoS Med 2005;2:e73.
5. Kobayashi S, Boggon TJ, Dayaram T, Janne PA, Kocher O, Meyerson M, et al. EGFR mutation and resistance of non-small-cell lung cancer to gefitinib. N Engl J Med 2005;352:786–92.
6. Engelman JA, Zejnullahu K, Mitsudomi T, Song Y, Hyland C, Park JO, et al. MET amplification leads to gefitinib resistance in lung cancer by activating ERBB3 signaling. Science 2007;316:1039–43.
7. Yano S, Wang W, Li Q, Matsumoto K, Sakurama H, Nakamura T, et al. Hepatocyte growth factor induces gefitinib resistance of lung adenocarcinoma with epidermal growth factor receptor-activating mutations. Cancer Res 2008;68:9479–87.
8. Turke AB, Zejnullahu K, Wu YL, Song Y, Dias-Santagata D, Lifshits E, et al. Preexistence and clonal selection of MET amplification in EGFR mutant NSCLC. Cancer Cell 2010;17:77–88.
9. Wang W, Li Q, Yamada T, Matsumoto K, Matsumoto I, Oda M, et al. Crosstalk to stromal fibroblasts induces resistance of lung cancer to epidermal growth factor receptor tyrosine kinase inhibitors. Clin Cancer Res 2009;15:6630–8.
10. Onitsuka T, Uramoto H, Nose N, Takenoyama M, Hanagiri T, Sugio K, et al. Acquired resistance to gefitinib: the contribution of mechanisms other than the T790M, MET, and HGF status. Lung Cancer 2010;68:198–203.
11. Matsumoto K, Nakamura T. Hepatocyte growth factor and the MET system as a mediator of tumor-stromal interactions. Int J Cancer 2006;119:477–83.
12. Raynaud FI, Eccles S, Clarke PA, Hayes A, Nutley B, Alix S, et al. Pharmacologic characterization of a potent inhibitor of class I phosphatidylinositide 3-kinases. Cancer Res 2007;67:5840–50.
13. Kong D, Yamori T. Phosphatidylinositol 3-kinase inhibitors: promising drug candidates for cancer therapy. Cancer Sci 2008;99:1734–40.
14. Engelman JA. Targeting PI3K signalling in cancer: opportunities, challenges and limitations. Nat Rev Cancer 2009;9:550–62.
15. Yamasaki F, Johansen MJ, Zhang D, Krishnamurthy S, Felix E, Bartholomeusz C, et al. Acquired resistance to erlotinib in A-431 epidermoid cancer cells requires down-regulation of MMAC1/PTEN and up-regulation of phosphorylated Akt. Cancer Res 2007;67:5779–88.
16. Ogino A, Kitao H, Hirano S, Uchida A, Ishiai M, Kozuki T, et al. Emergence of epidermal growth factor receptor T790M mutation during chronic exposure to gefitinib in a non small cell lung cancer cell line. Cancer Res 2007;67:7807–14.
17. Kharas MG, Janes MR, Scarfone VM, Lilly MB, Knight ZA, Shokat KM, et al. Ablation of PI3K blocks BCR-ABL leukemogenesis in mice, and a dual PI3K/mTOR inhibitor prevents expansion of human BCR-ABL+ leukemia cells. J Clin Invest 2008;118:3038–50.
18. Liu P, Cheng H, Roberts TM, Zhao JJ. Targeting the phosphoinositide 3-kinase pathway in cancer. Nat Rev Drug Discov 2009;8:627–44.
19. Inoue A, Suzuki T, Fukuhara T, Maemondo M, Kimura Y, Morikawa N, et al. Prospective phase II study of gefitinib for chemotherapy-naive patients with advanced non-small-cell lung cancer with epidermal growth factor receptor gene mutations. J Clin Oncol 2006;24:3340–6.
20. Yun CH, Mengwasser KE, Toms AV, Woo MS, Greulich H, Wong KK, et al. The T790M mutation in EGFR kinase causes drug resistance by increasing the affinity for ATP. Proc Natl Acad Sci U S A 2008;105:2070–5.
21. Nakamura T, Nishizawa T, Hagiya M, Seki T, Shimonishi M, Sugimura A, et al. Molecular cloning and expression of human hepatocyte growth factor. Nature 1989;342:440–3.
22. Green LM, Reade JL, Ware CF. Rapid colorimetric assay for cell viability: application to the quantitation of cytotoxic and growth inhibitory lymphokines. J Immunol Methods 1984;70:257–68.
23. Chou TC, Talalay P. Quantitative analysis of dose-effect relationships: the combined effects of multiple drugs or enzyme inhibitors. Adv Enzyme Regul 1984;22:27–55.
24. Faber AC, Li D, Song Y, Liang MC, Yeap BY, Bronson RT, et al. Differential induction of apoptosis in HER2 and EGFR addicted cancers following PI3K inhibition. Proc Natl Acad Sci U S A 2009;106:19503–8.
25. Yamada T, Matsumoto K, Wang W, Li Q, Nishioka Y, Sekido Y, et al. Hepatocyte growth factor reduces susceptibility to an irreversible epidermal growth factor receptor inhibitor in EGFR-T790M mutant lung cancer. Clin Cancer Res 2010;16:174–83.
26. Raynaud FI, Eccles SA, Patel S, Alix S, Box G, Chuckowree I, et al. Biological properties of potent inhibitors of class I phosphatidylinositide 3-kinases: from PI-103 through PI-540, PI-620 to the oral agent GDC-0941. Mol Cancer Ther 2009;8:1725–38.
27. Matsumoto K, Nakamura T. Mechanisms and significance of bifunctional NK4 in cancer treatment. Biochem Biophys Res Commun 2005;333:316–27.
28. Shah NP, Kasap C, Weier C, Balbas M, Nicoll JM, Bleickardt E, et al. Transient potent BCR-ABL inhibition is sufficient to commit chronic myeloid leukemia cells irreversibly to apoptosis. Cancer Cell 2008;14:485–93.
29. Kong D, Yamori T. Advances in development of phosphatidylinositol 3-kinase inhibitors. Curr Med Chem 2009;16:2839–54.
30. Dan S, Yoshimi H, Okamura M, Mukai Y, Yamori T. Inhibition of PI3K by ZSTK474 suppressed tumor growth not via apoptosis but G0/G1 arrest. Biochem Biophys Res Commun 2009;379:104–9.
31. Engelman JA, Chen L, Tan XH, Crosby K, Guimaraes AR, Upadhyay R, et al. Effective use of PI3K and MEK inhibitors to treat mutant Kras G12D and PIK3CA H1047R murine lung cancers. Nat Med 2008;14:1351–6.
32. Fan QW, Knight ZA, Goldenberg DD, Yu W, Mostov KE, Stokoe D, et al. A dual PI3 kinase/mTOR inhibitor reveals emergent efficacy in glioma. Cancer Cell 2006;9:341–9.
33. Sharma SV, Lee DY, Li B, Quinlan MP, Takahashi F, Maheswaran S, et al. A chromatin-mediated reversible drug-tolerant state in cancer cell subpopulations. Cell 2010;141:69–80.

BMP-9 induces proliferation of multiple types of endothelial cells in vitro and in vivo

Yuka Suzuki[1], Noritaka Ohga[2], Yasuyuki Morishita[1], Kyoko Hida[2], Kohei Miyazono[1] and Tetsuro Watabe[1,3,*]

[1]Department of Molecular Pathology, Graduate School of Medicine, University of Tokyo, Tokyo 113-0033, Japan
[2]Department of Oral Pathology and Biology, Division of Oral Pathological Science, Division of Vascular Biology, Graduate School of Dental Medicine, University of Hokkaido, Hokkaido 060-0808, Japan
[3]PRESTO, Japan Science Technology Agency, Kawaguchi, Saitama 332-0012, Japan
*Author for correspondence (t-watabe@umin.ac.jp)

Accepted 25 February 2010
Journal of Cell Science 123, 1684-1692

doi:10.1242/jcs.061556

Summary

Members of the bone morphogenetic protein (BMP) family have been implicated in the development and maintenance of vascular systems. Whereas members of the BMP-2/4 and osteogenic protein-1 groups signal via activin receptor-like kinase (ALK)-2, ALK-3 and ALK-6, BMP-9 and BMP-10 have been reported to bind to ALK-1 in endothelial cells. However, the roles of BMP-9–ALK-1 signaling in the regulation of endothelial cells have not yet been fully elucidated. Here, using various systems, we examined the effects of BMP-9 on the proliferation of endothelial cells. Vascular-tube formation from ex vivo allantoic explants of mouse embryos was promoted by BMP-9. BMP-9, as well as BMP-4 and BMP-6, also induced the proliferation of in-vitro-cultured mouse embryonic-stem-cell-derived endothelial cells (MESECs) by inducing the expression of vascular endothelial growth factor receptor 2 and Tie2, a receptor for angiopoietin-1. A decrease in ALK-1 expression or expression of constitutively active ALK-1 in MESECs abrogated and mimicked the effects of BMP-9 on the proliferation of MESECs, respectively, suggesting that BMP-9 promotes the proliferation of these cells via ALK-1. Furthermore, in vivo angiogenesis was promoted by BMP-9 in a Matrigel plug assay and in a BxPC3 xenograft model of human pancreatic cancer. Consistent with these in vivo findings, BMP-9 enhanced the proliferation of in-vitro-cultured normal endothelial cells from dermal tissues of adult mice and of tumor-associated endothelial cells isolated from tumor xenografts in host mice. These findings suggest that BMP-9 signaling activates the endothelium tested in the present study via ALK-1.

Key words: Embryonic stem cell, Allantois, Tumor angiogenesis, Pancreatic cancer, VEGFR2, Tie2

Introduction

Blood vessels consist of a lining of endothelial cells surrounded by mural cells (pericytes and vascular smooth muscle cells), and play essential roles in the maintenance of tissue homeostasis by carrying oxygen and nutrients to distant organs (Carmeliet, 2005). Defects in vascular systems thus result in many types of human disease. Hereditary hemorrhagic telangiectasia (HHT), also known as Osler-Weber-Rendu disease, is characterized by telangiectases in the nose, oral cavity and gastrointestinal tract, as well as arteriovenous malformations in multiple organs, including lung, liver and brain, which can result in severe ischemic injury or stroke (Shovlin et al., 2000). HHT is an autosomal dominant vascular disease, the majority of cases of which are caused by mutations in the gene for either activin receptor-like kinase (ALK)-1 (*ACVRL1*) or endoglin (*ENG*), which are a type-I receptor and co-receptor for members of the transforming growth factor (TGF)β family, respectively.

The TGFβ family consists of structurally related and multifunctional proteins, including TGFβs, activins, Nodal and bone morphogenetic proteins (BMPs) (Feng and Derynck, 2005). Members of the TGFβ family signal via heteromeric complexes of type II and type I serine/threonine kinase receptors. Upon ligand binding, the constitutively active type II receptor kinase phosphorylates the type I receptor, which in turn activates downstream signal transduction cascades, including Smad pathways. Activins and TGFβs bind to type I receptors known as ALK-4 and ALK-5, respectively. BMPs bind three BMP type I receptors (ALK-2, ALK-3 and ALK-6). The activated type I receptors phosphorylate receptor-regulated Smad proteins (R-Smads). Smad2 and Smad3 transduce signals for TGFβs, activins and Nodal, whereas Smad1, Smad5 and Smad8 are specific to signaling of BMPs (Miyazono et al., 2010). An exception to this is ALK-1, which is preferentially expressed in endothelial cells. ALK-1 binds TGFβ and activates the Smad1 and Smad5 pathways (Oh et al., 2000). Goumans and colleagues showed that TGFβ activates ALK-5–Smad2/3 and ALK-1–Smad1/5/8 pathways, leading to inhibition and activation of endothelial cell migration and proliferation, respectively (Goumans et al., 2002).

BMP-family members are subdivided into separate subgroups on the basis of similarity of primary amino acid sequence. They include the BMP-2/4 group (BMP-2 and BMP-4), osteogenic protein-1 (OP-1) group (BMP-5, BMP-6, BMP-7 and BMP-8) and BMP-9/10 group (BMP-9 and BMP-10) (Miyazono et al., 2010). BMP-9 has been shown to be highly expressed in fetal liver (Celeste et al., 1994) and in the liver of adult mice (Miller et al., 2000). BMP-9 exhibits growth-stimulatory effects on primary rat hepatocytes (Song et al., 1995), and has also been implicated in osteogenesis, chondrogenesis (Majumdar et al., 2001), glucose and fatty-acid metabolism (Chen et al., 2003), iron homeostasis (Truksa et al., 2006) and the differentiation of cholinergic neurons (López-Coviella et al., 2000).

Recent studies have shown that BMP-9 binds with high affinity to ALK-1 and endoglin in endothelial cells, and induces phosphorylation of Smad1 and/or Smad5 (Brown et al., 2005). This signaling inhibits basic fibroblast growth factor (FGF)-stimulated proliferation and migration of bovine aortic endothelial cells and vascular endothelial growth factor (VEGF)-induced

Journal of Cell Science

angiogenesis (Scharpfenecker et al., 2007). BMP-9 also inhibits the migration and growth of human dermal microvascular endothelial cells (HMVEC-ds) (David et al., 2007) and the DNA synthesis of human aortic endothelial cells (Upton et al., 2009) via ALK-1. Furthermore, BMP-9 is present in the circulating blood to maintain the maturation of blood vessels (David et al., 2008). These findings suggest that BMP-9 has inhibitory effects on endothelial cells, a conclusion that is not consistent with previous reports that TGFβ-mediated ALK-1 signaling activates endothelium (Goumans et al., 2002).

The development of the vascular system includes two distinct processes: vasculogenesis and angiogenesis (Coultas et al., 2005). During mouse embryogenesis, the initial development of vascular endothelium, termed vasculogenesis, occurs in the mesodermal layer of the yolk sac on embryonic day 7 (E7.0), yielding structures termed blood islands (E7.5-E8.5). The blood islands consist of endothelial progenitors termed angioblasts, which express VEGF receptor-2 (VEGFR2), which is also known as Flk1 (Kennedy et al., 1997; Nishikawa et al., 1998). In angiogenesis, new vessels sprout from the pre-existing vessels and are further remodeled to form mature blood vessels. In embryos, angiogenesis contributes to the establishment of hierarchical vascular trees after endothelial capillary networks have been formed by vasculogenesis. In adults, angiogenesis is essential for the repair and remodeling of tissues during wound healing and ischemia, and for the physiological female reproductive cycle. Neovascularization also plays a pivotal role in pathological processes such as tumor growth, chronic inflammation and diabetic vasculopathy.

Embryonic vascular differentiation has been recapitulated in an in-vitro-differentiation system from embryonic stem cells (ESCs) (Vittet et al., 1996; Hirashima et al., 1999; Yamashita et al., 2000). When VEGFR2-expressing (VEGFR2+) endothelial progenitors isolated from differentiation cultures are re-differentiated in the presence of VEGF, various endothelial markers are sequentially upregulated in a pattern similar to that observed in early embryos (Vittet et al., 1996). Using this system, we have previously shown that BMP-4 stimulates the proliferation and migration of endothelial cells via activation of VEGF–VEGFR2 and angiopoietin-1 (Ang-1)-Tie2 signaling in mouse embryonic-stem-cell-derived endothelial cells (MESECs) (Suzuki et al., 2008), whereas Kiyono and Shibuya (Kiyono and Shibuya, 2003) reported that BMP-4 induces apoptosis of capillary endothelial cells during rat pupillary-membrane regression. It is thus possible that BMP-9 has various effects depending on the cellular context.

In the present study, we examined the roles of BMP-9 in embryonic vascular development and adult angiogenesis. We found that the addition of BMP-9 to culture significantly promoted vasculogenesis of the allantois and induced proliferation of MESECs. Furthermore, we showed that BMP-9-induced proliferation was transduced via ALK-1. Finally, BMP-9 enhanced angiogenesis in Matrigel plug assays and pancreatic carcinoma xenografts in adult mice. These findings suggest that BMP-9 is capable of activating endothelium via ALK-1 and inducing vessel formation in vivo.

Results

Expression of components of the BMP-9 signaling pathway in E8.25 mouse embryos

We first examined whether the components of the BMP-9–ALK-1 signaling pathways are present in mouse embryos. The development of vascular systems in mouse embryos begins at E7.5, when VEGFR2+ endothelial progenitors initiate endothelial differentiation. At E8.5, the murine allantois, which lays down the umbilical vasculature that is critical for fetal survival and development, is formed and vascularizes intrinsically (Downs et al., 2001), rather than by angiogenesis involving the yolk sac or fetus. This tissue has therefore been used to study embryonic vessel formation.

E8.25 embryos were excised to obtain the allantois, which was subjected to semi-quantitative reverse transcriptase (RT)-PCR analyses. Endothelial and mural cells that differentiated from mouse ESCs (Yamashita et al., 2000; Watabe et al., 2003) were also examined for the expression of various BMP-9 signaling components. As shown in Fig. 1, expression of BMP-9 ligand was detected in allantoic, endothelial and mural cells. Furthermore, expression of type I receptors (ALK-2, ALK-3 and ALK-6) was also observed in all three samples (Fig. 1), whereas that of ALK-1 was restricted to the allantoic and endothelial cells, confirming endothelium-specific expression of ALK-1. Taken together with the findings that other BMP-related signaling components, including type II receptors (BMPR-II), R-Smads (Smad1, Smad5 and Smad8) and Co-Smad (Smad4), are expressed in the allantois (data not shown), these results suggest that signals mediated by BMP-9 are activated in the allantois of E8.25 embryos.

Induction of vessel formation by BMP-9 in ex vivo allantoic explants

Next, to examine the roles of BMP-9 in vasculogenesis and angiogenesis, we used an isolated allantois model (Downs et al., 2001). Excised allantoises from mouse E8.25 embryos were individually cultured in suspension for 2 days. When BMP-9 was added to the ex vivo culture, the PECAM1-positive area of allantoic explants was increased (Fig. 2A,B). However, the vessels formed in the presence of BMP-9 seemed disorganized and disconnected compared with the control (Fig. 2A). These findings suggest that BMP-9 promotes irregular formation of embryonic vascular vessels.

BMP-9 increases the number of MESECs

Because we observed pro-vasculogenic and -angiogenic effects of BMP-9 in an ex vivo culture system, we next examined the effects of BMP-9 signaling on embryonic endothelial cells with an in vitro

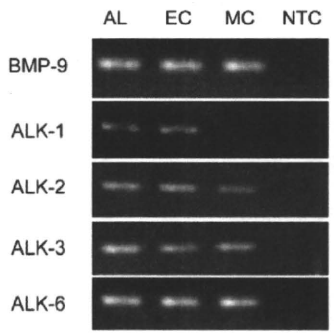

Fig. 1. Expression of BMP-related signaling components in allantoic explants. Allantoises (AL) were excised from E8.25 mouse embryos and subjected to semi-quantitative RT-PCR analyses for BMP-9, ALK-1, ALK-2, ALK-3 and ALK-6. Endothelial cells (EC) and mural cells (MC) were obtained by in vitro differentiation of CCE mouse ESCs and were also subjected to RT-PCR analysis for comparison of expression with that in allantois. NTC, no template control.

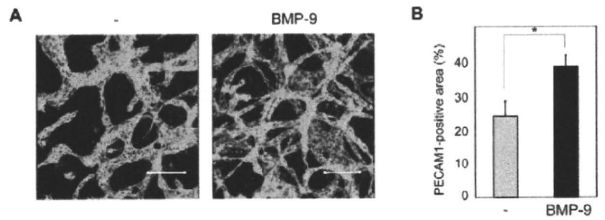

Fig. 2. Effects of BMP-9 on vessel formation from allantoic explants. (**A**) Allantoises were excised from E8.25 embryos and cultured in the absence (–) or presence of BMP-9 (4 ng/ml), followed by immunostaining for PECAM1 (green). Scale bars: 100 μm. (**B**) Percent PECAM1-positive area. Each value represents the mean of seven fields. Error bars, s.d. *$P<0.00004$.

vascular differentiation system from mouse ESCs (Yamashita et al., 2000; Watabe et al., 2003). VEGFR2+ endothelial progenitor cells derived from ESCs differentiate predominantly into endothelial cells when cultured in serum-free SFO medium in the presence of VEGF. When BMP-9 was added to culture of VEGFR2+ cells, the number of endothelial cells obtained was significantly increased and their sheet formation was significantly inhibited (Fig. 3A,B), which is similar to our previous finding that BMP-4, a member of the BMP-2/4 group, significantly increases the number of MESECs (Suzuki et al., 2008) (Fig. 3B).

When BMP-6, a member of the OP-1 group, was tested in this proliferation assay, it also increased the number of MESECs (Fig. 3B). These findings suggest that members of all three BMP subfamilies are capable of promoting the proliferation of embryonic endothelial cells during differentiation from VEGFR2+ progenitor cells.

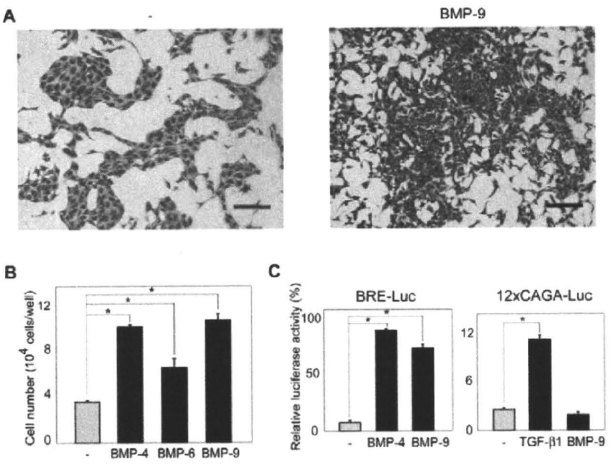

Fig. 3. Effects of BMP-9 on the number of MESECs. (**A**,**B**) VEGFR2+ cells (5×10^4/well) derived from CCE cells were cultured in serum-free SFO medium containing 30 ng/ml of VEGF in the absence (–) or presence of BMP-4 (60 ng/ml), BMP-6 (360 ng/ml) or BMP-9 (1 ng/ml) for 2 days, followed by photography (A; '–' and BMP-9) and determination of cell numbers (B). Scale bars: 200 μm. (**C**) Luciferase promoter assays were carried out using MESECs to determine whether BMP-9 activates BMP-related (BRE-Luc) or TGFβ-related (12×CAGA-Luc) intracellular signaling pathways. BMP-4 (60 ng/ml) and TGFβ1 (1 ng/ml) were used as controls for BRE-Luc and 12×CAGA-Luc, respectively. Error bars, s.d. *$P<0.006$.

BMPs activate the Smad1/5/8 signaling axis, whereas TGFβ, activins and Nodal activate the Smad2/3 signaling axis. To determine which intracellular Smad signaling pathways are activated by BMP-9 in MESECs, we carried out luciferase reporter assays using promoter reporter constructs that specifically respond to each signal. As shown in Fig. 3C, BMP-9 activated BMP–Smad1/5/8-specific (BRE-Luc) but not TGFβ–Smad2/3-specific (12×CAGA) reporter constructs, which were activated by BMP-4 and TGFβ, respectively. We also examined whether the concentrations of BMPs used in the proliferation assay activate the Smad1/5/8 signaling pathways at comparable levels. Activation of Smad1/5/8 signaling pathways can also be monitored by the expression level of Id1, a faithful target of BMP signaling (Valdimarsdottir et al., 2002). As shown in supplementary material Fig. S1, BMP-4, BMP-6 and BMP-9 induced Id1 expression to a similar relative extent as they enhanced the proliferation of MESECs (Fig. 3B). These findings suggest that activation of BMP-9 increases the number of MESECs by activating Smad1/5/8 signaling pathways.

Specific inhibition of the effects of BMP-9 on MESEC proliferation by soluble ALK-1

Although all members of the BMP family exhibit similar effects on endothelial cell proliferation, BMP-9 and BMP-10 have been reported to utilize ALK-1, whereas BMP-4 and BMP-6 bind ALK-2, ALK-3 and ALK-6 (David et al., 2007; Scharpfenecker et al., 2007). To examine whether the BMP-9 used in the assay preferentially binds to ALK-1 on MESECs, we used soluble chimeric receptors containing extracellular domains of ALK-1 and ALK-3 (ALK-1-Fc and ALK-3-Fc, respectively). As shown in Fig. 4A, ALK-1-Fc inhibited the BMP-9-mediated increase in number of MESECs, whereas control-Fc or ALK-3-Fc did not. These findings suggest that BMP-9 binds to ALK-1 with higher affinity than to ALK-3 in MESECs.

Increase of ALK-1 expression during endothelial differentiation

Although ALK-1 has been shown to be preferentially expressed in endothelial cells, its expression during endothelial differentiation from ESC-derived vascular progenitors has not been elucidated. We therefore examined the expression of ALK-1, ALK-3 and vascular markers over time during in vitro differentiation of ESC-derived VEGFR2+ cells. The expression of PECAM1, an endothelial marker, began to increase from 12 hours after stimulation with VEGF in the absence of serum (Fig. 4B) (Kawasaki et al., 2008). The level of expression of ALK-1 in VEGF-stimulated ESC-derived progenitor cells was similar to that of PECAM1, whereas that of endoglin increased earlier than those of PECAM1 and ALK-1. By contrast, ALK-3 expression was detected in the VEGFR2+ endothelial progenitors and decreased during endothelial differentiation. Although these findings need to be confirmed at protein levels, they suggest that ALK-1 signals mediated by BMP-9 are activated after endothelial cells are differentiated from ESC-derived VEGFR2+ cells, whereas ALK-3 signals mediated by BMP-4 can be activated in VEGFR2+ progenitor cells.

Essential role of ALK-1 in the BMP-9-mediated increase in number of MESECs

Although BMP-9 was shown to bind preferentially to ALK-1, it remains unclear whether the BMP-9-induced increase in the number